

# Prescribed chattering reduction control for quadrotors using aperiodic signal updating

Xiaohui Yue<sup>a,b</sup>, Xingling Shao<sup>a,b\*</sup>, Jie Li<sup>a,b</sup>

(a. Key Laboratory of Instrumentation Science & Dynamic Measurement, Ministry of Education, North University of China, Taiyuan 030051, China b. National Key Laboratory for Electronic Measurement Technology, School of Instrument and Electronics, North University of China, Taiyuan 030051, China)

---

## Abstract

In the paper, a prescribed chattering reduction control using aperiodic signal updating is presented for quadrotors subject to parameter uncertainties and external disturbances. Using estimation errors instead of tracking errors to update adaptive laws, estimator-based minimum learning parameter (EMLP) observers capable of relaxing computational complexity are respectively explored in translational and rotational loops to reject fast time-varying disturbances, such that transient oscillations can be efficiently mitigated even with a large adaptive gain. Meanwhile, quantitative analysis for transient learning performance is characterized by means of  $L_2$  norms of time differential of neural network weights. With the aid of disturbance estimates, a relative event-triggered robust control law is derived by inserting a compensation term to guarantee a favorable trajectory tracking with Zeno free behaviors and decreased sampling cost. Besides, an appointed-time prescribed performance control (APPC) is established, enforcing trajectory tracking errors to evolve within pre-given regions even in face of triggering errors, where a piecewise and continuous finite-time behavior function, rather than an exponential decaying function, is applied to enable a preassigned fast convergence time without retuning controller parameters. Finally, the stability of closed-loop system is proved via Lyapunov synthesis, while comparative studies are provided to validate the effectiveness of presented control method.

**Keywords:** estimator-based minimum learning parameter, quadrotors, appointed-time prescribed performance control, event-triggered.

---

## 1. Introduction

Quadrotors have been viewed as extremely important autonomous vehicles with numerous applications due to rapid maneuverability, simple structure and low manufacturing cost, which are extensively embodied in scenarios of transporting [1], [22], surveillance [6], search and rescue [7]. In recent years, a variety of studies on motion control for quadrotors has been conducted to allow for a reliable and effective task execution, such as path following [8], [10], trajectory tracking [3], [11] and attitude maneuvering [2], [12], [13]. Particularly, trajectory tracking has become a central research focus, since it is an enabling technique for successful implementation of sophisticated aerospace missions. However, arising from inherent characteristics of quadrotor system formulated as under-actuated and nonlinearity, and the presence of unknown environment disturbances pose great challenges to the development of high-performance quadrotor controllers.

To enhance system robustness against unknown uncertainties, abundant control algorithms have been reported for quadrotors, to name a few, sliding mode control in [14]-[16], extended-state-observer-based control in [17], [18] and neural network (NN) control in [19]-[21]. Wherein, NN control is treated as a powerful model free data-driven solution to recover exogenous disturbances from recorded data, owing to its universal generalized features. In [22], radial basis function neural networks (RBFNNs) are developed for a class of uncertain stochastic nonlinear systems to online approximate the unknown continuous functions and by fusing **dynamic surface control (DSC)** technology, iterative differential operations of virtual control signals are avoided. As expatiated in [23], an adaptive control scheme is proposed for quadrotors via the help of differential NNs, where Lyapunov stability theory is employed to prove that both tracking and estimation errors are bounded. To improve anti-interference property, an adaptive robust controller equipped with RBFNNs is presented in [24] for nonlinear bilateral teleoperation manipulators. However, it can be found that the current NN approaches [22]-[24] may suffer from the issue of learning explosion, which is attributed to the need of updating excessive neural elements for high-precision estimation results, especially as the enlargement in the dimension of input arguments of functions to be learned. Aiming at this problem, a minimal learning parameter (MLP) principle [25], [26] is discussed, the major difference towards the traditional NNs lies in that the learning dimension of weight vector is reduced to one. The fact avoids a time-consuming learning process, such that real-time response capability of system can be preserved. In [25], with the aid of a MLP, a neural-approximation-based robust adaptive control method is interviewed for flexible air-breathing hypersonic vehicles

in the presence of parametric uncertainties to ensure exploited controller with a low computational load. Similarly, by combining a MLP with sliding mode control strategy, an adaptive neural sliding mode controller is established in [26] for micro electro mechanical systems subject to time-varying disturbances. Note that for aforementioned results in [22]-[26], it is typically recommended to select a large adaptive gain in NN to accelerate learning rate against uncertainties and further narrow steady-state error boundaries, while in turn oscillations during the transient inevitably aggravate as adaptive gains increase, giving rise to physical actuators exceeding their allowable ranges and deteriorated tracking performances, particularly in the presence of nonzero initial tracking errors. Thus, it is of high values to investigate a chattering reduction fast learning scheme preserving a reduced computational complexity for quadrotors. In addition, note that although uniformly ultimately bounded (UUB) results are available in [23]-[26], performance specifications such as convergence time, maximum overshoots and steady-state precision are not explicitly taken into account in the previous controller realization, leading to a design conservatism in enforcing constraints satisfaction, i.e., controller parameters are always entailed to be repeatedly tuned in a trial and error manner to hold predesigned specifications, which is unfeasible and inconvenient in some cases with severe unknown uncertainties.

Prescribed performance control (PPC) proposed in [27], aims to avoid tedious parameter tuning process via transforming a constrained error dynamics into an unconstrained one with equivalent error transformation and appropriate performance function. Recently, PPC technology has received tremendous attentions from control communities. For instance, a decentralized robust controller is explored in [28] for Multi-Agents considering uncertain system dynamics and external disturbances, where PPC is introduced to impose predetermined constraints on system responses. In [29], a modified PPC-based neural controller is exploited for air-breathing hypersonic vehicles, which guarantees transient tracking errors with arbitrarily small overshoots. Under the framework of backstepping, an adaptive control scheme with prescribed performance constrains is presented in [30] for quadrotors to characterize preselected convergence rate and overshoot for position states by a strict-feedback means. In [31], a leader-follower control scheme with guaranteed properties is interviewed for nonholonomic mobile robots, such that UUB results can be obtained without incurring collision between each robot. Nevertheless, in these studies, although prescribed tracking regions can be regulated as a prior, due to the employment of exponential performance function, it can only ensure tracking errors evolve within a predefined boundary and converge to ultimate steady-state values with an exponential decaying rate, i.e., infinite prescribed time is always imposed for the existing PPC results [27]-[31], which greatly hinder its applications in cases of tighter time limits. To remedy such drawback, an appointed-time prescribed performance control (APPC) is exploited for spacecrafts in [32], where via constructing a piecewise and continuous finite-time behavior profile as a novel performance function, guaranteed properties with a finite prescribed time can be easily governed by users in advance. In [33], an appointed-time stable control protocol is explored for second-order Multi-Agent systems considering time-varying disturbances, while APPC is synthesized to characterize a finite prescribed time and restrain tracking errors within the preset region. However, it is still open to apply APPC to address specification constraints for quadrotors to obtain an optimal convergent rate, and it should be stressed that the available reports regarding PPC [27]-[33] are designed based on time-triggered control mechanisms, implying that periodic signal sampling is needed no matter system demands or not, causing a significant waste of computational resources, which is harmful to deal with micro-digital platform based quadrotor systems with limited computational and storage capabilities.

Interestingly, aperiodic sampling strategy provides a promising solution to save constrained onboard resources and prevailing methods include quantization [34], [35] and event-triggered [4], [36]-[39]. In particular, event-triggered control method, by which the signals can be transmitted only when the designed triggering condition is violated, has been intensively employed in various control systems. By incorporating a relative threshold event-triggered approach, an adaptive sliding mode control scheme for nonlinear systems is proposed in [36] to reduce transmission load. In [37], a finite-time robust control law with a fixed threshold event-triggered condition is established for second-order Multi-Agent systems, which greatly saves the network communication resources in controller-to-actuator channels. In [38], under the premise of excluding Zeno phenomenon, an event-based neural network controller based on a fixed threshold is synthesized for autonomous surface vehicles to achieve aperiodic signal updating. Note that these event-triggered control approaches

can diminish resource consumption to a favorable level, but few results are available for quadrotors due to its nonlinear, under-actuated and intricate coupling natures. Consequently, to employ an event-triggered mechanism to quadrotor systems is meaningful for extending operational range and enhancing mission efficiency.

Stimulated by the aforementioned investigations, a prescribed chattering reduction control for quadrotors using aperiodic signal updating is proposed, whose superiorities can be summarized as follows:

- 1) Different from the developed control methods for quadrotors [11], [17], where objectives are only to enhance anti-interference capability of the whole system, the proposed neural control scheme is devoted to simultaneously improve anti-interference capability, reduce onboard power consumption, along with a guaranteed control performance. Obviously, the above properties are main concerns in practice, which greatly affect mission completion efficiency of quadrotors.
- 2) In contrast to the traditional RBFNNs [22], [24], [40], [41] suffering from transient oscillations and learning explosion in the presence of a sizable adaptive gain, an estimator-based minimal learning parameter (EMLP) observer is proposed for quadrotors to simultaneously obtain a competitive estimation performance with reduced learning complexity and transient oscillations. To be specific, adaptive weight updating laws are calculated using estimation errors rather than tracking errors that widely applied in [25], [26], enabling a decoupling of learning and control loops if the observer bandwidth is chosen sufficiently large than that of control loop, and a reduced chattering degree in learning behaviors even with a large adaptive gain can be expected. As far as learning complexity is concerned, as opposed to the reported neural approximation schemes [22]-[24], [40], [41] that demand updating each element of weight vector, herein, inspired by MLP, only one adaptive parameter is needed to learn online for each subsystem, greatly diminishing computational burden. Moreover, by using  $L_2$  norms of the differential of NN weights to quantify transient performances, a rigorous mathematical deduction shows that the presented EMLP observer can generate smaller oscillations than the traditional RBFNNs.
- 3) Compared with the standard PPC solutions [27]-[31], [42], [43], where infinite time is required to ensure system responses to reach the final values, the designed APPC with a piecewise and continuous finite-time behavior function is established, such that a fast prescribed time can be predetermined via tuning design parameter  $T$ . In addition, different from the current finite-time controller studies [5], [44], where settling time relies on initial conditions and controller parameters, a fast convergence rate can be arbitrarily preassigned by APPC without depending on initial states and tuning controller parameters repeatedly.
- 4) Unlike the existing time-triggered controller designs for quadrotors [6]-[17], [45], [46], which require a high sampling frequency to maintain a satisfactory tracking performance, leading to a mass of computational resources dissipation, the proposed resource-aware control strategy using an event-triggered mechanism associated with the magnitude of control actions is devised to acquire a competitive tracking accuracy with a reduced sampling cost, where a relative event-triggered condition is used to determine the updating time instants of control signals, allowing for a less triggering burden compared with continuous and fixed threshold event-triggered methods [37], [38], [47], especially when the control behavior varies within a large region.

## 2. Preliminaries and Problem Formulation

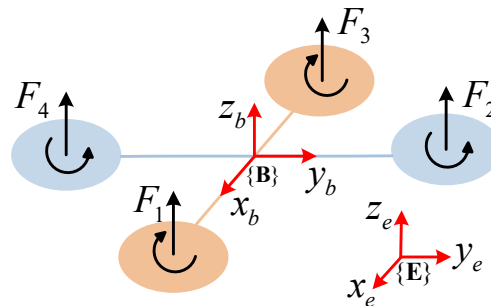


Fig.1 Schematic diagram of quadrotors

## 2.1 Quadrotor model

To facilitate analysis and illustration for the quadrotor dynamics, Fig.1 shows the configuration of the quadrotor, where a body-fixed frame  $\{\mathbf{B}\}$  and an earth-fixed inertial frame  $\{\mathbf{E}\}$  are respectively framed. Here, as seen from Fig.1, the thrust  $F_m (m=1,2,3,4)$  generated by the rotation of corresponding propeller can steer the position and orientation of the quadrotor. Resorting to [46], the motion of quadrotors can be formulated by the subsequent kinematics and dynamics:

$$\begin{cases} \dot{\mathbf{p}} = \mathbf{v} \\ \dot{\mathbf{v}} = \mathbf{f}_v(\mathbf{v}) + \mathbf{F}(\Theta, u_F) + \mathbf{d}_v \\ \dot{\Theta} = \omega \\ \dot{\omega} = \mathbf{f}_\omega(\omega) + \mathbf{g}_\omega \mathbf{u} + \mathbf{d}_\omega \end{cases} \quad (1)$$

where  $\mathbf{p} = [p_x, p_y, p_z]^T$  and  $\mathbf{v} = [v_x, v_y, v_z]^T$  represent the position and linear velocity of quadrotors in  $\{\mathbf{E}\}$ ,  $\Theta = [\Theta_\phi, \Theta_\theta, \Theta_\psi]^T$  and  $\omega = [\omega_\phi, \omega_\theta, \omega_\psi]^T$  determine the attitude angle and angular velocity in  $\{\mathbf{B}\}$ . The nonlinear functions correlated with parametric uncertainties are calculated by  $\mathbf{f}_v(\mathbf{v}) = -\mathbf{\Pi}_v \mathbf{v}/m$  and  $\mathbf{f}_\omega(\omega) = -\mathbf{J}^{-1} \mathbf{\Pi}_\omega \omega$ , where both  $\mathbf{\Pi}_v = \text{diag}\{\Pi_{v,x}, \Pi_{v,y}, \Pi_{v,z}\}$  and  $\mathbf{\Pi}_\omega = \text{diag}\{\Pi_{\omega,\phi}, \Pi_{\omega,\theta}, \Pi_{\omega,\psi}\}$  are deemed as the unknown damping matrices, and  $m$  indicates the mass of the quadrotor, and  $\mathbf{J} = \text{diag}\{J_\phi, J_\theta, J_\psi\}$  denotes the positive diagonal matrix with  $J_\phi, J_\theta, J_\psi$  being the rotational inertias. The virtual control input of translational subsystem can be derived by  $\mathbf{F}(\Theta, u_F) \triangleq (\mathbf{K}u_F - \mathbf{G})/m$  while  $\mathbf{K} = [\cos(\Theta_\psi) \sin(\Theta_\theta) \cos(\Theta_\phi) + \sin(\Theta_\psi) \sin(\Theta_\theta) \sin(\Theta_\phi), \sin(\Theta_\psi) \sin(\Theta_\theta) \cos(\Theta_\phi) - \cos(\Theta_\psi) \sin(\Theta_\theta) \sin(\Theta_\phi), \cos(\Theta_\theta) \cos(\Theta_\phi)]^T$  is applied to achieve the conversion from body frame to inertial frame, and  $\mathbf{G} = [0, 0, mg]^T$  with  $g$  being the gravitational acceleration constant. Control inputs  $u_F$ ,  $\mathbf{u} = [u_\phi, u_\theta, u_\psi]^T$  are considered as the applied thrust force and torques.  $\mathbf{g}_\omega = \text{diag}\{l/J_\phi, l/J_\theta, c/J_\psi\}$  is a diagonal constant matrix, where  $l, c$  respectively stand for the distance from each propeller to the center of the mass of the quadrotor and force-to-moment factor. Besides, it should be pointed that there exist the following equivalent relationships between control inputs and rotor thrust described in Fig.1:  $u_F = F_1 + F_2 + F_3 + F_4$ ,  $u_\phi = F_2 - F_4$ ,  $u_\theta = F_3 - F_1$ ,  $u_\psi = F_1 - F_2 + F_3 - F_4$ .  $\mathbf{d}_v = [d_x, d_y, d_z]^T$  and  $\mathbf{d}_\omega = [d_\phi, d_\theta, d_\psi]^T$  are unknown but bounded environmental perturbations.

**Assumption 1** [47]: Consider the reference signals  $p_k^d(t), k = x, y, z$  as sufficiently smooth functions, which indicates that  $p_k^d(t), \dot{p}_k^d(t), \ddot{p}_k^d(t)$  all are bounded. Thus, there exists a constant  $D_0 > 0$  over a compact set  $\Omega_0$  satisfying

$$\left[ p_k^d, \dot{p}_k^d, \ddot{p}_k^d \right]^T \in \Omega_0 = \left\{ \left[ p_k^d, \dot{p}_k^d, \ddot{p}_k^d \right]^T : (p_k^d)^2 + (\dot{p}_k^d)^2 + (\ddot{p}_k^d)^2 \leq D_0 \right\} \subset \mathbf{R}^3 \quad (2)$$

## 2.2 RBFNN

Generally, for any given continuous function  $f(\cdot)$  on a compact set, if node number  $L$  is sufficiently large, there exists an ideal weight vector  $\mathbf{w}^* = [w_1^*, w_2^*, \dots, w_L^*]^T \in \mathbf{R}^L$  such that

$$f(\mathbf{x}_m) = \mathbf{w}^{*T} \mathbf{a}(\mathbf{x}_m) + \varepsilon(\mathbf{x}_m) \quad (3)$$

where  $\mathbf{x}_m = [x_1, x_2, \dots, x_m]^T \in \Omega_x \subset \mathbf{R}^m$  denotes the input vector with  $m$  being number of the input elements.  $\mathbf{w}^*$  is the ideal weight and  $L > 1$  represents the node number of the hidden layer.  $\varepsilon(\mathbf{x}_m)$  denotes reconstruction error fulfilling  $|\varepsilon(\mathbf{x}_m)| \leq \bar{\varepsilon}$  with  $\bar{\varepsilon} > 0$  being a constant. The vector  $\mathbf{a}(\mathbf{x}_m) = [\alpha_1(\mathbf{x}_m), \alpha_2(\mathbf{x}_m), \dots, \alpha_L(\mathbf{x}_m)]^T$  is the basis function, where  $\alpha_j$  stands for Gaussian basis function and can be described as

$$\alpha_j(\mathbf{x}_m) = \exp\left(\frac{-\|\mathbf{x}_m - \delta\|^2}{2b_j^2}\right), j = 1, 2, \dots, L \quad (4)$$

where  $\delta = [\delta_1, \delta_2, \dots, \delta_m]^T$  is the center vector and  $b_j$  denotes the width.

**Remark 1:** It should be noteworthy that the exponential function  $\exp(\cdot) > 0$  can keep increasing monotonously, and consider the exponential term  $-\|\mathbf{x}_m - \delta\|^2 / 2b_j^2 \leq 0$  in (4), one has  $0 < \alpha_j(\mathbf{x}_m) \leq 1$ . Therefore, the Gaussian basis function is bounded, i.e.,  $\|\mathbf{a}(\mathbf{x}_m)\| \leq \bar{\alpha}$  with  $\bar{\alpha}$  being a positive constant. Attributed to the application of numerous hidden units to identify unknown functions with a high precision, traditional NN methods inevitably possess the issue of learning

explosion. Besides, as argument vector dimension of the observed function increases, the number of parameters to be regulated will drastically grow, which brings in a heavy computational complexity for quadrotors.

### 2.3 PPC

By virtue of imposing boundary constraints on tracking errors, PPC realizes a prior regulation of system responses with regard to convergence rate, transient overshoot and steady-state accuracy. Consider a generalized tracking error  $e(t)$  satisfying the following inequality:

$$-\underline{\lambda}K(t) < e(t) < \bar{\lambda}K(t), \forall t \geq 0 \quad (5)$$

where  $K(t)$  represents a prescribed performance function, while  $-\underline{\lambda}K(t), \bar{\lambda}K(t)$  are boundary constraints with  $\underline{\lambda}, \bar{\lambda} \in (0,1]$  being positive design parameters. Referring to [48],  $K(t)$  can be expressed as below:

$$K(t) = (K_0 - K_\infty)\exp(-\ell t) + K_\infty \quad (6)$$

with  $K_0, K_\infty$  being initial and steady-state values of the performance function, respectively.  $\ell$  is a positive design parameter applied to steer convergence rate of  $K(t)$ . In addition, to ensure the crucial role of PPC in implementation of controller, initial restricted condition  $-\underline{\lambda}K(0) < e(0) < \bar{\lambda}K(0)$  cannot be transgressed.

**Remark 2:** Under a PPC paradigm, performance function can only reach the predesigned final value with a pre-given exponential speed, which means that tracking error boundaries  $-\underline{\lambda}K(t), \bar{\lambda}K(t)$  lack a capability of arriving at specified values within an appointed time. But from the aspect of engineering practice, since executing complicated missions with a limited reaching time is usually a basic requirement, relevant tasks may be affected and even fail if a desired tracking performance cannot be achieved before the mission-given time.

**Control objective:** The objective of this study for quadrotors is to synthesize a prescribed event-triggered control law with chattering reduction such that

- 1) All the signals involved within the closed-loop control framework can realize UUB results despite of modeling nonlinearities, parameter uncertainties and external disturbances.
- 2) Trajectory tracking errors conform to  $-\underline{\Sigma}_k \chi_k(t) \leq e_{p,k}(t) \leq \bar{\Sigma}_k \chi_k(t), \forall t \geq 0$  within a preassigned prescribed time, where a finite-time preselected performance function herein is defined as  $\chi_k(t)$ , which is elaborately introduced in Section 3.2.
- 3) Zeno phenomenon, i.e., there exist infinite discrete transitions in a finite time, can be excluded.

### 3. Main Results

In this section, a prescribed chattering reduction control for quadrotors is proposed as shown in Fig. 3, where an APPC is constructed to make sure that trajectory tracking error converges to a predefined region with a finite-time prescribed time, and an EMLP observer is presented to counteract uncertainties arising from parameter uncertainties and external disturbances, such that oscillations at transient and heavy computational burden can be mitigated. Besides, an event-triggered robust control law based on a relative threshold is established to determine the communication schedule of control actions for quadrotors. Then, a DSC is introduced at each step to address the issue of ‘‘explosion of complexity’’ induced by the repeated differentials of virtual control signals.

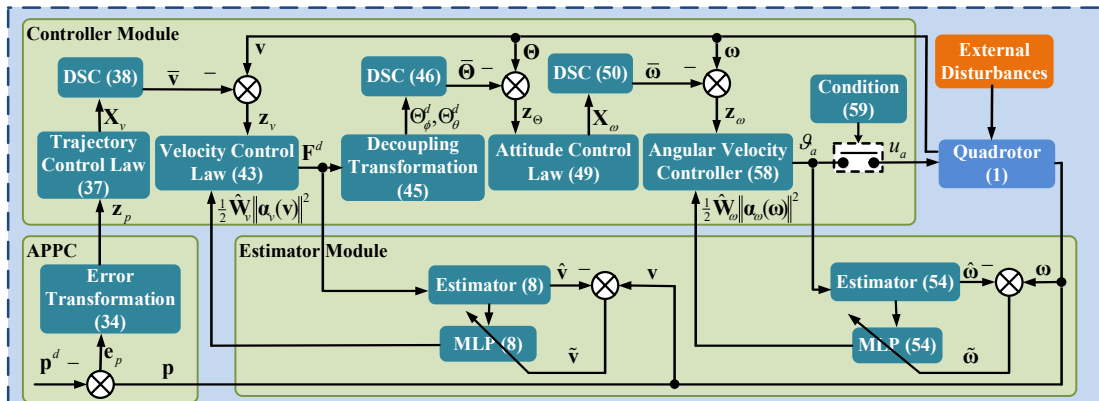


Fig. 2 Structure diagram of presented controller

### 3.1 EMLP observer

In the subsection, to illustrate the design principle of presented EMLP observer, take the translational dynamics as an example to express the essential philosophy. Here, by virtue of MLP [25], [26], the lumped disturbances  $\Delta_v \triangleq \mathbf{f}_v(\mathbf{v}) + \mathbf{d}_v$  existing in quadrotors can be approximated as follows:

$$\Delta_v = \frac{1}{2} \mathbf{W}_v^* \|\mathbf{a}_v(\mathbf{v})\|^2 + \boldsymbol{\varepsilon}_v(\mathbf{v}) \quad (7)$$

where the ideal weight vector  $\mathbf{W}_v^* = [W_{v,x}^*, W_{v,y}^*, W_{v,z}^*]^T$  with each element being  $W_{v,k}^* = \|\mathbf{w}_{v,k}^*\|^2 e_{v,k}$ ,  $k = x, y, z$ , while  $e_{v,k}$  is velocity tracking error. And according to [25], there exists a positive constant  $\bar{W}$  such that  $\|\mathbf{W}_v^*\| \leq \bar{W}$ .  $\mathbf{a}_v(\mathbf{v})$  is a basis function of NN,  $\mathbf{v} = [v_x, v_y, v_z]^T$  is the input data and  $\boldsymbol{\varepsilon}_v = [\varepsilon_{v,x}, \varepsilon_{v,y}, \varepsilon_{v,z}]^T$  is the reconstruction error.

**Remark 3:** Revisiting traditional RBFNN in Section 2.2, it can be found that a time-consuming learning process is inevitable, particularly when excessive nodes of hidden layer are employed to ensure a high-precision identification result. Here, only a learning parameter is regulated online for each subsystem. As a consequence, by using MLP technology, a low computational complexity can be guaranteed irrespective of the number of hidden neural nodes in NN.

Aiming at identifying  $\Delta_v$  to migrate the negative effect, an EMLP observer consisting of a state estimator and an adaptive weight updating law is constructed as below:

$$\begin{cases} \dot{\hat{\mathbf{v}}} = \mathbf{F}(\boldsymbol{\Theta}, u_F) + \frac{1}{2} \hat{\mathbf{W}}_v \|\mathbf{a}_v(\mathbf{v})\|^2 + \kappa_v \tilde{\mathbf{v}}, \hat{\mathbf{v}}(0) = \mathbf{v}(0) \\ \dot{\hat{\mathbf{W}}}_v = \frac{1}{2} \eta_v \left[ \|\mathbf{a}_v(\mathbf{v})\|^2 \tilde{\mathbf{v}} - \sigma_v \hat{\mathbf{W}}_v \right] \end{cases} \quad (8)$$

where  $\hat{\mathbf{W}}_v$  is an estimate of ideal weight vector  $\mathbf{W}_v^*$ .  $\tilde{\mathbf{v}} = \mathbf{v} - \hat{\mathbf{v}}$  denotes velocity estimation error vector with  $\hat{\mathbf{v}}$  being the estimate. Notations  $\kappa_v, \eta_v$  and  $\sigma_v$  are positive design parameters, which respectively determine observer bandwidth, adaptive gain and modification parameter.

Combined with quadrotor dynamics(1), lumped disturbances (7) along with EMLP observer(8), then error dynamics of velocity estimation and weight updating can be integrated as

$$\begin{cases} \dot{\tilde{\mathbf{v}}} = \frac{1}{2} \tilde{\mathbf{W}}_v \|\mathbf{a}_v(\mathbf{v})\|^2 - \kappa_v \tilde{\mathbf{v}} + \boldsymbol{\varepsilon}_v(\mathbf{v}) \\ \dot{\tilde{\mathbf{W}}}_v = -\frac{1}{2} \eta_v \left[ \|\mathbf{a}_v(\mathbf{v})\|^2 \tilde{\mathbf{v}} - \sigma_v \tilde{\mathbf{W}}_v \right] \end{cases} \quad (9)$$

with  $\tilde{\mathbf{W}}_v = \mathbf{W}_v^* - \hat{\mathbf{W}}_v$ .

Then, in order to explain and demonstrate the improved transient learning performance, the truncated  $L_2$  norm of the differential of NN weight is calculated to measure chattering degrees of the EMLP estimation results, which corresponds to frequency features and can be expressed by  $\|\dot{\tilde{\mathbf{W}}}_v\|_{L_2, t^*} = \int_0^{t^*} \|\dot{\tilde{\mathbf{W}}}_v\| dt$ . Note that a bigger  $L_2$  norm of the differential of NN weight indicates more oscillations involved in the system response. Thus, an improved transient performance yields if the proposed EMLP observer can derive a smaller  $\|\dot{\tilde{\mathbf{W}}}_v\|_{L_2, t^*}$  than classical RBFNN approach.

**Theorem 1:** Taking the estimation error dynamics (9) into consideration, and provided that  $2\kappa_v - 1 \geq \mu_T, \sigma_v/2 \geq \mu_T$  with  $\mu_T$  being a positive constant, it follows that  $\|\dot{\tilde{\mathbf{W}}}_v\|_{L_2, t^*}$  conforms to

$$\|\dot{\tilde{\mathbf{W}}}_v\|_{L_2, t^*} \leq \frac{\eta_v \bar{\alpha}^2}{\sqrt{2(2\kappa_v - 1)}} \left( \|\tilde{\mathbf{v}}(0)\| + \frac{\|\tilde{\mathbf{W}}_v(0)\|}{\sqrt{\eta_v}} + \sqrt{2\sigma_v t^*} \right) + \frac{\eta_v \sigma_v}{\sqrt{2}} \left( \bar{W} + \sqrt{\eta_v} \left( \sqrt{\frac{2\sigma_v}{\mu_T}} + \|\tilde{\mathbf{v}}(0)\| \right) + \|\tilde{\mathbf{W}}_v(0)\| \right) \sqrt{t^*} \quad (10)$$

**Proof:** Establish a Lyapunov function as follows:

$$V = \frac{1}{2} \tilde{\mathbf{v}}^T \tilde{\mathbf{v}} + \frac{1}{2\eta_v} \tilde{\mathbf{W}}_v^T \tilde{\mathbf{W}}_v \quad (11)$$

Recalling (9), the time differential of (11) is expressed as

$$\begin{aligned}\dot{V} &= \tilde{\mathbf{v}}^T \left( \frac{1}{2} \tilde{\mathbf{W}}_v \|\mathbf{a}_v(\mathbf{v})\|^2 - \kappa_v \tilde{\mathbf{v}} + \boldsymbol{\varepsilon}_v(\mathbf{v}) \right) - \frac{1}{2} \tilde{\mathbf{W}}_v^T \left[ \|\mathbf{a}_v(\mathbf{v})\|^2 \tilde{\mathbf{v}} - \sigma_v \hat{\mathbf{W}}_v \right] = -\kappa_v \|\tilde{\mathbf{v}}\|^2 + \frac{1}{2} \sigma_v \tilde{\mathbf{W}}_v^T \hat{\mathbf{W}}_v + \tilde{\mathbf{v}}^T \boldsymbol{\varepsilon}_v(\mathbf{v}) \\ &= -\kappa_v \|\tilde{\mathbf{v}}\|^2 + \frac{1}{2} \sigma_v \tilde{\mathbf{W}}_v^T (\mathbf{W}_v^* - \tilde{\mathbf{W}}_v) + \tilde{\mathbf{v}}^T \boldsymbol{\varepsilon}_v(\mathbf{v}) = -\kappa_v \|\tilde{\mathbf{v}}\|^2 - \frac{1}{2} \sigma_v \|\tilde{\mathbf{W}}_v\|^2 + \frac{1}{2} \sigma_v \tilde{\mathbf{W}}_v^T \mathbf{W}_v^* + \tilde{\mathbf{v}}^T \boldsymbol{\varepsilon}_v(\mathbf{v})\end{aligned}\quad (12)$$

On the basis of Young's inequality [51], one has

$$\|\tilde{\mathbf{W}}_v^T \mathbf{W}_v^*\| \leq \frac{1}{2} \|\tilde{\mathbf{W}}_v\|^2 + \frac{1}{2} \|\mathbf{W}_v^*\|^2 \leq \frac{1}{2} \|\tilde{\mathbf{W}}_v\|^2 + \frac{1}{2} \bar{W}^2, \quad \|\tilde{\mathbf{v}}^T \boldsymbol{\varepsilon}_v(\mathbf{v})\| \leq \frac{1}{2} \|\tilde{\mathbf{v}}\|^2 + \frac{1}{2} \|\boldsymbol{\varepsilon}_v(\mathbf{v})\|^2 \leq \frac{1}{2} \|\tilde{\mathbf{v}}\|^2 + \frac{1}{2} \bar{\varepsilon}^2 \quad (13)$$

Substituting the results of (13) into (12), it further produces that

$$\dot{V} \leq -\left( \kappa_v - \frac{1}{2} \right) \|\tilde{\mathbf{v}}\|^2 - \frac{1}{4} \sigma_v \|\tilde{\mathbf{W}}_v\|^2 + \varpi_T \quad (14)$$

where  $\varpi_T = \sigma_v \bar{W}^2 / 4 + \bar{\varepsilon}^2 / 2$ , and only when the following inequalities are satisfied:

$$2\kappa_v - 1 \geq \mu_T, \quad \frac{1}{2} \sigma_v \geq \mu_T \quad (15)$$

with  $\mu_T$  being a positive constant, (14) can be rewritten as

$$\dot{V} \leq -\mu_T V + \varpi_T \quad (16)$$

Then, taking the integral of both sides of (16) gives

$$V \leq \frac{\varpi_T}{\mu_T} (1 - e^{-\mu_T t}) + V(0) e^{-\mu_T t} \quad (17)$$

Following the chosen Lyapunov function (11) and applying  $\sqrt{a+b} \leq \sqrt{a} + \sqrt{b}, a \geq 0, b \geq 0$ , one has

$$\|\tilde{\mathbf{v}}\| \leq \sqrt{\frac{2\varpi_T}{\mu_T}} + \|\tilde{\mathbf{v}}(0)\| + \frac{\|\tilde{\mathbf{W}}_v(0)\|}{\sqrt{\eta_v}}, \quad \|\tilde{\mathbf{W}}_v\| \leq \sqrt{\eta_v} \left( \sqrt{\frac{2\varpi_T}{\mu_T}} + \|\tilde{\mathbf{v}}(0)\| \right) + \|\tilde{\mathbf{W}}_v(0)\| \quad (18)$$

According to (14) and considering that  $\sigma_v$  is a positive scalar, we can further derive that

$$\left( \kappa_v - \frac{1}{2} \right) \|\tilde{\mathbf{v}}\|^2 \leq -\dot{V} - \frac{1}{4} \sigma_v \|\tilde{\mathbf{W}}_v\|^2 + \varpi_T \leq -\dot{V} + \varpi_T \quad (19)$$

Subsequently, integrating both sides of (19) over  $(0, t^*]$ , we have

$$\|\tilde{\mathbf{v}}\|_{L_2, t^*}^2 \leq \frac{2(V(0) + \varpi_T t^*)}{2\kappa_v - 1} \quad (20)$$

Based on (20), it further produces

$$\|\tilde{\mathbf{v}}\|_{L_2, t^*} \leq \frac{1}{\sqrt{2\kappa_v - 1}} \left( \|\tilde{\mathbf{v}}(0)\| + \frac{\|\tilde{\mathbf{W}}_v(0)\|}{\sqrt{\eta_v}} + \sqrt{2\varpi_T t^*} \right) \quad (21)$$

Aiming at quantitatively describing transient performances of EMLP observer, one can further calculate the upper bound of  $\|\dot{\hat{\mathbf{W}}}_v\|$ . In order to obtain the result, via (8), it yields

$$\|\dot{\hat{\mathbf{W}}}_v\| \leq \frac{1}{2} \eta_v \left[ \|\mathbf{a}_v(\mathbf{v})\|^2 \|\tilde{\mathbf{v}}\| + \sigma_v \|\hat{\mathbf{W}}_v\| \right] \quad (22)$$

According to Remark 1, (18) along with (22), it follows that

$$\|\dot{\hat{\mathbf{W}}}_v\| \leq \frac{1}{2} \eta_v \left[ \bar{\alpha}^2 \|\tilde{\mathbf{v}}\| + \sigma_v (\bar{W} + \sqrt{\eta_v} \left( \sqrt{\frac{2\varpi_T}{\mu_T}} + \|\tilde{\mathbf{v}}(0)\| \right)) + \|\tilde{\mathbf{W}}_v(0)\| \right] \quad (23)$$

which on the basis of  $(a+b)^2 \leq 2(a^2 + b^2)$  leads to

$$\|\dot{\hat{\mathbf{W}}}_v\|^2 \leq \frac{1}{4} \eta_v^2 \left[ \bar{\alpha}^2 \|\tilde{\mathbf{v}}\| + \sigma_v \left( \bar{W} + \sqrt{\eta_v} \left( \sqrt{\frac{2\varpi_T}{\mu_T}} + \|\tilde{\mathbf{v}}(0)\| \right) + \|\tilde{\mathbf{W}}_v(0)\| \right) \right]^2 \leq \frac{1}{2} \eta_v^2 \left[ \bar{\alpha}^4 \|\tilde{\mathbf{v}}\|^2 + \sigma_v^2 \left( \bar{W} + \sqrt{\eta_v} \left( \sqrt{\frac{2\varpi_T}{\mu_T}} + \|\tilde{\mathbf{v}}(0)\| \right) + \|\tilde{\mathbf{W}}_v(0)\| \right)^2 \right] \quad (24)$$

Integrating both sides of (24) over  $(0, t^*]$  and utilizing  $\sqrt{a+b} \leq \sqrt{a} + \sqrt{b}, a \geq 0, b \geq 0$  results in

$$\left\| \dot{\tilde{\mathbf{W}}}_v \right\|_{L_2, t^*}^2 \leq \frac{1}{2} \eta_v^2 \left[ \bar{\alpha}^4 \|\tilde{\mathbf{v}}\|_{L_2, t^*}^2 + \sigma_v^2 (\bar{W} + \sqrt{\eta_v} \left( \sqrt{\frac{2\sigma_T}{\mu_T}} + \|\tilde{\mathbf{v}}(0)\| \right) + \|\tilde{\mathbf{W}}_v(0)\|)^2 t^* \right] \quad (25)$$

In connection with upper bound of (21), the truncated  $L_2$  norm of  $\left\| \dot{\tilde{\mathbf{W}}}_v \right\|$  can be derived as follows:

$$\left\| \dot{\tilde{\mathbf{W}}}_v \right\|_{L_2, t^*} \leq \frac{\eta_v \bar{\alpha}^2}{\sqrt{2(2\kappa_v - 1)}} \left( \|\tilde{\mathbf{v}}(0)\| + \frac{\|\tilde{\mathbf{W}}_v(0)\|}{\sqrt{\eta_v}} + \sqrt{2\sigma_T t^*} \right) + \frac{\eta_v \sigma_v}{\sqrt{2}} \left( \bar{W} + \sqrt{\eta_v} \left( \sqrt{\frac{2\sigma_T}{\mu_T}} + \|\tilde{\mathbf{v}}(0)\| \right) + \|\tilde{\mathbf{W}}_v(0)\| \right) \sqrt{t^*} \quad (26)$$

Afterwards, to make a comparison with the existing RBFNN in Section 2.2, we introduce the following Lemma 1.

**Lemma 1** [51]: Define velocity tracking error as  $\mathbf{e}_v$  and construct the adaptive weight updating law of classical RBFNN

as  $\dot{\hat{\mathbf{M}}}_v = \eta_v [\mathbf{a}_v(\mathbf{v}) \mathbf{e}_v^T - \sigma_v \hat{\mathbf{M}}_v]$ . Then,  $\left\| \dot{\hat{\mathbf{M}}}_v \right\|_{L_2, t^*}$  conforms to

$$\left\| \dot{\hat{\mathbf{M}}}_v \right\|_{L_2, t^*} \leq \frac{\sqrt{2\eta_v} \bar{\alpha}}{\sqrt{2\kappa_v - 1}} \left( \|\mathbf{e}_v(0)\| + \frac{\|\tilde{\mathbf{M}}_v(0)\|}{\sqrt{\eta_v}} + \sqrt{2\sigma_T t^*} \right) + \sqrt{2\eta_v} \sigma_v \left( \bar{W} + \sqrt{\eta_v} \left( \sqrt{\frac{2\sigma_T}{\mu_T}} + \|\mathbf{e}_v(0)\| \right) + \|\tilde{\mathbf{M}}_v(0)\| \right) \sqrt{t^*} \quad (27)$$

**Remark 4:** It is found from (10) and (27) that  $\left\| \dot{\tilde{\mathbf{W}}}_v \right\|_{L_2, t^*}$  and  $\left\| \dot{\hat{\mathbf{M}}}_v \right\|_{L_2, t^*}$  will get large when adaptive gains increase, and thus, transient oscillations aggravate for not only RBFNN approach, but also for EMLP observer. However, in contrast to the existing NN schemes, the presented EMLP observer provides two extra design freedoms to alleviate oscillations under the same adaptive gain. One is that by setting  $\mathbf{v}(0) = \hat{\mathbf{v}}(0)$ , EMLP observer effectively removes the undesired transient learning process induced by nonzero initial tracking errors. Another is that estimation error  $\tilde{\mathbf{v}}$ , rather than tracking error  $\mathbf{e}_v$ , is employed to update adaptive law, by which control and learning loops can be decoupled if observer bandwidth  $\kappa_v$  is chosen as 2 to 3 times larger than control gain  $k_v$ . Note that a larger observer bandwidth will lead to transient property with less chattering. As a result, EMLP observer permits a relatively higher adaptive gain compared with classical NN approximators. Evidently, the above two superiorities cannot be provided by the current NN methods.

### 3.2 APPC

To guarantee a preassigned fast convergence time, a piecewise and continuous finite-time behavior function is designed as below:

$$\chi_k(t) = \begin{cases} \left[ \frac{(T-t)}{T} \right]^{1-\tilde{h}} (\chi_{k0} - \chi_{k\infty}) + \chi_{k\infty}, & 0 \leq t < T \\ \chi_{k\infty}, & t \geq T \end{cases} \quad (28)$$

where prescribed time  $T$  is used to regulate the reaching time of performance function.  $\tilde{h} \in (0, 1)$  determines the slope of performance function at transient.  $\chi_{k0}, \chi_{k\infty}$  are initial and final values of  $\chi_k(t)$ , which respectively limit transient overshoot and maximal steady-state allowable values.

**Theorem 2:** For any given prescribed time  $T > 0$ , the developed performance function  $\chi_k(t)$  is monotonously decreasing for  $0 \leq t < T$  and fulfills  $\dot{\chi}_k(t) = 0$  as  $t \geq T$ . Moreover, both  $\chi_k(t)$  and its differential  $\dot{\chi}_k(t)$  are continuous and bounded.

**Proof:** As  $0 \leq t < T$ , time differential of  $\chi_k(t)$  is calculated as

$$\begin{aligned} \dot{\chi}_k(t) &= -\frac{1}{T(1-\tilde{h})} \left[ \frac{(T-t)}{T} \right]^{\tilde{h}} (\chi_{k0} - \chi_{k\infty}) = -\frac{1}{T(1-\tilde{h})} \left\{ \left[ \frac{(T-t)}{T} \right]^{1-\tilde{h}} (\chi_{k0} - \chi_{k\infty}) \right\}^{\tilde{h}} (\chi_{k0} - \chi_{k\infty})^{1-\tilde{h}} \\ &= -\frac{1}{T(1-\tilde{h})} \left\{ \left[ \frac{(T-t)}{T} \right]^{1-\tilde{h}} (\chi_{k0} - \chi_{k\infty}) + \chi_{k\infty} - \chi_{k\infty} \right\}^{\tilde{h}} (\chi_{k0} - \chi_{k\infty})^{1-\tilde{h}} = -\frac{(\chi_{k0} - \chi_{k\infty})^{1-\tilde{h}}}{T(1-\tilde{h})} (\chi_k(t) - \chi_{k\infty})^{\tilde{h}} \end{aligned}$$

and  $0 \leq t < T$ , it follows that

$$\dot{\chi}_k(t) = 0$$

Then, time differential of (28) can be given as

$$\dot{\chi}_k(t) = \begin{cases} -\frac{(\chi_{k0} - \chi_{k\infty})^{1-h}}{T(1-h)}(\chi_k(t) - \chi_{k\infty})^h, & 0 \leq t < T \\ 0, & t \geq T \end{cases} \quad (29)$$

Obviously,  $\chi_k(t)$  is monotonic decreasing over  $[0, T)$  and  $\chi_k(t)$  remains invariable over  $[T, \infty)$ , resulting in that  $\chi_k(\infty) \leq \chi_k(t) \leq \chi_k(0)$ . It can be followed from (28) that  $\chi_k(0) = \chi_{k0}$ ,  $\chi_k(\infty) = \chi_{k\infty}$ . Consequently,  $\chi_k(t)$  on its domain of definition is bounded.

Additionally, following (29), we can obtain that

$$\lim_{t \rightarrow T^-} \dot{\chi}_k(t) = \lim_{t \rightarrow T^+} \dot{\chi}_k(t) = \dot{\chi}_k(T) = 0 \quad (30)$$

which means that  $\dot{\chi}_k(t)$  is continuous on  $\forall t \in [0, \infty)$ . Resorting to the boundedness properties of continuous function on a closed interval, one can derive that  $\dot{\chi}_k(t)$  is a bounded function.

The proof of Theorem 2 is completed.

**Remark 5:** Fig. 3 illustrates comparison of convergence performance of behavior functions between PPC and APPC, where  $K(0) = \chi_k(0) = 7$ ,  $K(\infty) = \chi_k(\infty) = 0.5$ . For PPC, performance function  $K(t)$  in (6) is evidently deficient in arriving at the final value within a finite time. Differently, by tuning parameter  $T$ ,  $\chi_k(t)$  can reach user-designed steady-state values within limited times, which provides a more user-friendly and appropriate option for practical implementations with time-specified requirement.

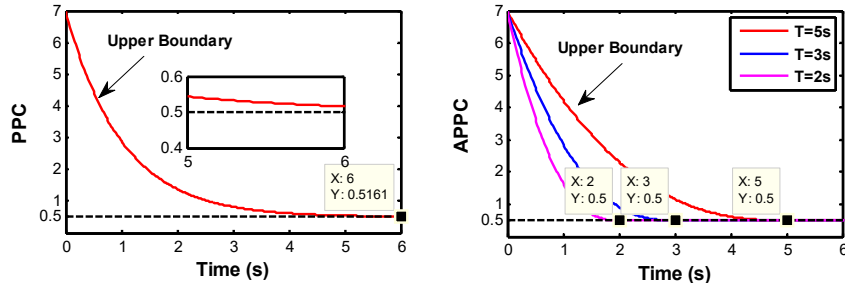


Fig.3 Comparison of convergence performance of behavior functions between PPC and APPC

Define trajectory tracking error as  $e_{p,k} = p_k - p_k^d$ ,  $k = x, y, z$ , where  $p_k^d$  represents reference signal. Similar to PPC, aiming at guaranteeing trajectory tracking errors without violating prescribed boundaries, the following restriction condition should be satisfied:

$$-\underline{\aleph}_k \chi_k(t) \leq e_{p,k}(t) \leq \bar{\aleph}_k \chi_k(t), \forall t \in [0, \infty) \quad (31)$$

where both  $\underline{\aleph}_k \in (0, 1]$  and  $\bar{\aleph}_k \in (0, 1]$  being positive design parameters.

Consider that it is tedious to directly devise an output constrained controller meeting (31), following PPC principle, to ensure that trajectory tracking errors can be restricted within the predetermined boundaries, the following equivalent error transformation is established:

$$e_{p,k}(t) = \chi_k(t) \Gamma(z_{p,k}(t)) \quad (32)$$

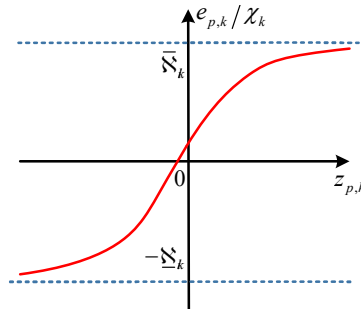


Fig. 4 Error transformed function  $\Gamma(\bullet)$

Apparently, based on (31), error transformed function  $\Gamma(z_k(t))$  should satisfy  $\lim_{z_k \rightarrow -\infty} \Gamma(z_k) = -\underline{\Sigma}_k$ ,  $\lim_{z_k \rightarrow \infty} \Gamma(z_k) = \bar{\Sigma}_k$ . Since  $\Gamma(z_{p,k})$  is a strictly monotonous increasing function in term of  $z_{p,k}$  and conforms to  $\Gamma(0) \neq 0$ . For convenience, as displayed in Fig.4,  $\Gamma(z_k(t))$  is typically selected as

$$\Gamma(z_{p,k}(t)) = \frac{\bar{\Sigma}_k \cdot \exp(z_{p,k}(t)) - \underline{\Sigma}_k \cdot \exp(-z_{p,k}(t))}{\exp(z_{p,k}(t)) + \exp(-z_{p,k}(t))} \quad (33)$$

Taking the inverse of (33), we can obtain

$$z_{p,k}(t) = \Gamma_k^{-1} \left( \frac{e_{p,k}(t)}{\chi_k(t)} \right) = \frac{1}{2} \ln \left( \frac{\underline{\Sigma}_k + e_{p,k}(t)/\chi_k(t)}{\bar{\Sigma}_k - e_{p,k}(t)/\chi_k(t)} \right) \quad (34)$$

whose derivative with time can be derived as

$$\dot{z}_{p,k}(t) = B_{p,k}(t)(\dot{e}_{p,k}(t) - \dot{\chi}_k(t)e_{p,k}(t)/\chi_k(t)) = B_{p,k}(t)(v_k(t) - \dot{p}_k^d(t) - \dot{\chi}_k(t)e_{p,k}(t)/\chi_k(t)) \quad (35)$$

with  $B_{p,k}(t) = \frac{1}{2\chi_k(t)} \left( \frac{1}{e_{p,k}(t)/\chi_k(t) + \underline{\Sigma}_k} - \frac{1}{e_{p,k}(t)/\chi_k(t) - \bar{\Sigma}_k} \right)$ . Note that transformed error  $z_k(t)$  is also called as the barrier function, which possesses the feature of finite escape whenever trajectory tracking error  $e_{p,k}(t)$  approaches the boundaries of the open set  $(-\underline{\Sigma}_k\chi_k, \bar{\Sigma}_k\chi_k)$ , that is,  $z_{p,k} \rightarrow -\infty$  as  $e_{p,k}/\chi_k \rightarrow -\underline{\Sigma}_k$ ,  $z_{p,k} \rightarrow \infty$  as  $e_{p,k}/\chi_k \rightarrow \bar{\Sigma}_k$ . Hence, by guaranteeing the boundedness of  $z_{p,k}$ , time-varying constrains imposed on  $e_{p,k}$  are not violated.

**Lemma 2** [27]: If error dynamics  $z_{p,k}$  is bounded over time domain  $[0, \infty)$  together with the condition  $-\bar{\Sigma}_k\chi_k(0) \leq e_k(0) \leq \underline{\Sigma}_k\chi_k(0)$  holds, trajectory tracking error  $e_k(t)$  will fulfill (31).

### 3.3 Controller design

**Step 1:** To stabilize  $z_{p,k}$ , we design virtual control law based on (35) as follows:

$$\mathbf{X}_{v,k}(t) = -k_p B_{p,k}^{-1}(t) z_{p,k}(t) + \dot{p}_k^d(t) + \frac{\dot{\chi}_k(t)e_{p,k}(t)}{\chi_k(t)}, \quad k = x, y, z \quad (36)$$

which can further be expressed as a compact vector form:

$$\mathbf{X}_v(t) = -k_p \mathbf{B}_p^{-1}(t) \mathbf{z}_p(t) + \dot{\mathbf{p}}^d(t) + \frac{\dot{\chi}(t)\mathbf{e}_p(t)}{\chi(t)} \quad (37)$$

where  $k_p$  is a positive control gain.  $\mathbf{B}_p = \text{diag}\{B_{p,x}, B_{p,y}, B_{p,z}\}$ ,  $\mathbf{z}_p(t) = [z_{p,x}, z_{p,y}, z_{p,z}]^T$ ,  $\mathbf{p}^d(t) = [p^d, p^d, p^d]^T$ ,  $\chi(t) = [\chi_x, \chi_y, \chi_z]^T$ ,  $\mathbf{e}_p(t) = [e_{p,x}, e_{p,y}, e_{p,z}]^T$ .

Next, a DSC technology is introduced to deal with the issue of ‘‘explosion of complex’’ induced by analytical differential, where first-order filter is constructed to obtain  $\dot{\bar{\mathbf{v}}}(t)$ :

$$\boldsymbol{\tau}_v \dot{\bar{\mathbf{v}}}(t) + \bar{\mathbf{v}}(t) = \mathbf{X}_v(t), \quad \bar{\mathbf{v}}(0) = \mathbf{X}_v(0) \quad (38)$$

where  $\boldsymbol{\tau}_v = \text{diag}\{\tau_{v,x}, \tau_{v,y}, \tau_{v,z}\}$  with  $\tau_{v,x}, \tau_{v,y}, \tau_{v,z}$  being time constants, and  $\bar{\mathbf{v}}(t)$  denotes an estimate vector of  $\mathbf{X}_v$ .

Define the surface error as

$$\boldsymbol{\varsigma}_v(t) = \bar{\mathbf{v}}(t) - \mathbf{X}_v(t) \quad (39)$$

Subsequently, differentiating  $\boldsymbol{\varsigma}_v(t)$  with regard to time produces

$$\dot{\boldsymbol{\varsigma}}_v(t) = \dot{\bar{\mathbf{v}}}(t) - \dot{\mathbf{X}}_v(t) = -\boldsymbol{\tau}_v^{-1} \boldsymbol{\varsigma}_v(t) - \dot{\mathbf{X}}_v(t) = -\boldsymbol{\tau}_v^{-1} \boldsymbol{\varsigma}_v(t) + \mathbf{Q}_v(\dot{\mathbf{z}}_p, \dot{\mathbf{p}}^d, \dot{\mathbf{e}}_p) \quad (40)$$

where  $\mathbf{Q}_v(\dot{\mathbf{z}}_p, \dot{\mathbf{p}}^d, \dot{\mathbf{e}}_p) = \mathbf{k}_p \dot{\mathbf{z}}_p(t) + \dot{\mathbf{p}}^d(t) + \dot{\boldsymbol{\Xi}}(t)$  and  $\boldsymbol{\Xi}(t) = \dot{\chi}(t)\mathbf{e}_p(t)/\chi(t)$ .

**Step 2:** Regard  $\bar{\mathbf{v}}$  as the reference command of linear velocity, then the tracking error in velocity loop can be written as

$$\mathbf{z}_v(t) = \mathbf{v}(t) - \bar{\mathbf{v}}(t) \quad (41)$$

Recalling (1), the time differential of  $\mathbf{z}_v(t)$  is formulated as

$$\dot{\mathbf{z}}_v(t) = \dot{\mathbf{v}}(t) - \dot{\bar{\mathbf{v}}}(t) = \mathbf{f}_v(\mathbf{v}) + \mathbf{F}(\boldsymbol{\Theta}, u_F) + \mathbf{d}_v - \dot{\bar{\mathbf{v}}}(t) \quad (42)$$

To realize velocity error stabilization, we design the following velocity controller by utilizing the identification results of EMLP observer:

$$\mathbf{F}^d(\boldsymbol{\Theta}^d, u_F) = -k_v \mathbf{z}_v(t) - \frac{1}{2} \hat{\mathbf{W}}_v \|\mathbf{a}_v(\mathbf{v})\|^2 + \dot{\mathbf{v}}(t) \quad (43)$$

where  $k_v$  is a positive control gain, and  $\mathbf{F}^d(\boldsymbol{\Theta}^d, u_F)$  corresponds to the virtual control signal.

It should be noted that the orientation of  $\mathbf{F}^d(\boldsymbol{\Theta}^d, u_F)$  can be regulated by the desired body attitude vector  $\boldsymbol{\Theta}^d = [\Theta_\phi^d, \Theta_\theta^d, \Theta_\psi^d]^T$  with  $\Theta_\phi^d, \Theta_\theta^d, \Theta_\psi^d$  respectively being desired roll, pitch and yaw. According to the coupling feature of quadrotors involved in (1), the components of  $\mathbf{F}^d(\boldsymbol{\Theta}^d, u_F) = [F_x^d, F_y^d, F_z^d]^T$  satisfy

$$\begin{cases} F_x^d = \frac{u_F}{m} (\cos(\Theta_\psi^d) \sin(\Theta_\theta^d) \cos(\Theta_\phi^d) + \sin(\Theta_\psi^d) \sin(\Theta_\phi^d)) \\ F_y^d = \frac{u_F}{m} (\sin(\Theta_\psi^d) \sin(\Theta_\theta^d) \cos(\Theta_\phi^d) - \cos(\Theta_\psi^d) \sin(\Theta_\phi^d)) \\ F_z^d = \frac{u_F}{m} (\cos(\Theta_\theta^d) \cos(\Theta_\phi^d)) - g \end{cases} \quad (44)$$

By inverse transformation of (44), it produces

$$\begin{cases} u_F = m \sqrt{(F_x^d)^2 + (F_y^d)^2 + (F_z^d + g)^2} \\ \Theta_\phi^d = \arcsin(m(F_x^d \sin(\Theta_\psi^d) - F_y^d \cos(\Theta_\psi^d)) / u_F) \\ \Theta_\theta^d = \arctan((F_x^d \cos(\Theta_\psi^d) + F_y^d \sin(\Theta_\psi^d)) / (F_z^d + g)) \end{cases} \quad (45)$$

where  $\Theta_\psi^d$  is offline given by some experienced manipulator. Note that by utilizing the quantitative relationship in (45), the quadrotor system can be decoupled into translational subsystem with slow dynamics and rotational subsystem with fast dynamics.

Then, aiming at circumventing tedious differential operations, it follows that first-order filter is framed as follows:

$$\boldsymbol{\tau}_\Theta \dot{\bar{\boldsymbol{\Theta}}}(t) + \bar{\boldsymbol{\Theta}}(t) = \boldsymbol{\Theta}^d(t), \quad \bar{\boldsymbol{\Theta}}(0) = \boldsymbol{\Theta}^d(0) \quad (46)$$

where  $\boldsymbol{\tau}_\Theta = \text{diag}\{\tau_{\Theta_\phi}, \tau_{\Theta_\theta}, \tau_{\Theta_\psi}\}$  with  $\tau_{\Theta_\phi}, \tau_{\Theta_\theta}, \tau_{\Theta_\psi}$  being time constants, while  $\bar{\boldsymbol{\Theta}}(t)$  stands for an estimate of  $\boldsymbol{\Theta}^d(t)$ .

Similar to the process in (40), differentiating the surface error  $\boldsymbol{\zeta}_\Theta(t) = \bar{\boldsymbol{\Theta}}(t) - \boldsymbol{\Theta}^d(t)$  with respect to time results in

$$\dot{\boldsymbol{\zeta}}_\Theta(t) = \dot{\bar{\boldsymbol{\Theta}}}(t) - \dot{\boldsymbol{\Theta}}^d(t) = -\boldsymbol{\tau}_\Theta^{-1} \boldsymbol{\zeta}_\Theta(t) - \dot{\boldsymbol{\Theta}}^d(t) = -\boldsymbol{\tau}_\Theta^{-1} \boldsymbol{\zeta}_\Theta(t) + \mathbf{Q}_\Theta(\dot{\boldsymbol{\Theta}}^d) \quad (47)$$

**Step 3:** For the sake of design of latter attitude control law, we consider  $\bar{\boldsymbol{\Theta}}(t)$  as attitude command and define attitude tracking error as  $\mathbf{z}_\Theta(t) = \boldsymbol{\Theta}(t) - \bar{\boldsymbol{\Theta}}(t)$ . Here, time differential of  $\mathbf{z}_\Theta(t)$  along (1) can be described by

$$\dot{\mathbf{z}}_\Theta(t) = \dot{\boldsymbol{\Theta}}(t) - \dot{\bar{\boldsymbol{\Theta}}}(t) \quad (48)$$

On the basis of (48), a virtual control law is devised:

$$\mathbf{X}_\omega(t) = -k_\Theta \mathbf{z}_\Theta(t) + \dot{\bar{\boldsymbol{\Theta}}}(t) \quad (49)$$

where  $k_\Theta$  is a positive control gain.

Following the DSC technology, we have

$$\boldsymbol{\tau}_\omega \dot{\bar{\boldsymbol{\omega}}}(t) + \bar{\boldsymbol{\omega}}(t) = \mathbf{X}_\omega(t), \quad \bar{\boldsymbol{\omega}}(0) = \mathbf{X}_\omega(0) \quad (50)$$

where  $\boldsymbol{\tau}_\omega = \text{diag}\{\tau_{\omega_\phi}, \tau_{\omega_\theta}, \tau_{\omega_\psi}\}$  with  $\tau_{\omega_\phi}, \tau_{\omega_\theta}, \tau_{\omega_\psi}$  are time constants, and  $\bar{\boldsymbol{\omega}} = [\bar{\omega}_\phi, \bar{\omega}_\theta, \bar{\omega}_\psi]^T$  is an estimate of  $\mathbf{X}_\omega$ .

Next, define the surface error as

$$\boldsymbol{\zeta}_\omega(t) = \bar{\boldsymbol{\omega}}(t) - \mathbf{X}_\omega(t) \quad (51)$$

whose time differential can be derived as

$$\dot{\boldsymbol{\zeta}}_\omega(t) = \dot{\bar{\boldsymbol{\omega}}}(t) - \dot{\mathbf{X}}_\omega(t) = -\boldsymbol{\tau}_\omega^{-1} \boldsymbol{\zeta}_\omega(t) - \dot{\mathbf{X}}_\omega(t) = -\boldsymbol{\tau}_\omega^{-1} \boldsymbol{\zeta}_\omega(t) + \mathbf{Q}_\omega(\dot{\mathbf{z}}_\Theta(t), \ddot{\bar{\boldsymbol{\Theta}}}(t)) \quad (52)$$

where  $\mathbf{Q}_\omega(\dot{\mathbf{z}}_\Theta(t), \ddot{\bar{\boldsymbol{\Theta}}}(t)) = k_\Theta \dot{\mathbf{z}}_\Theta(t) - \ddot{\bar{\boldsymbol{\Theta}}}(t)$ .

**Step 4:** The lumped disturbances in the rotational loop can be expressed in the following form:

$$\Delta_\omega = \mathbf{f}_\omega(\boldsymbol{\omega}) + \mathbf{d}_\omega = \frac{1}{2} \mathbf{W}_\omega^* \|\mathbf{a}_\omega(\boldsymbol{\omega})\|^2 + \boldsymbol{\varepsilon}_\omega(\boldsymbol{\omega}) \quad (53)$$

where  $\boldsymbol{\varepsilon}_\omega(\boldsymbol{\omega}) = [\varepsilon_{\omega,\phi}, \varepsilon_{\omega,\theta}, \varepsilon_{\omega,\psi}]^T$  means a reconstructed error vector. Then, to approximate  $\mathbf{W}_\omega^*$ , in line with (8), the adaptive update law in angular velocity loop can be given by

$$\begin{cases} \dot{\hat{\boldsymbol{\omega}}} = \mathbf{g}_\omega \mathbf{u} + \frac{1}{2} \hat{\mathbf{W}}_\omega \|\boldsymbol{\alpha}_\omega(\boldsymbol{\omega})\|^2 + \kappa_\omega \tilde{\boldsymbol{\omega}}, \hat{\boldsymbol{\omega}}(0) = \boldsymbol{\omega}(0) \\ \dot{\tilde{\mathbf{W}}}_\omega = \frac{1}{2} \eta_\omega \left[ \|\boldsymbol{\alpha}_\omega(\boldsymbol{\omega})\|^2 \tilde{\boldsymbol{\omega}} - \sigma_\omega \hat{\mathbf{W}}_\omega \right] \end{cases} \quad (54)$$

and estimation error dynamics can be calculated as

$$\begin{cases} \dot{\tilde{\boldsymbol{\omega}}} = \frac{1}{2} \tilde{\mathbf{W}}_\omega \|\boldsymbol{\alpha}_\omega(\boldsymbol{\omega})\|^2 - \kappa_\omega \tilde{\boldsymbol{\omega}} + \boldsymbol{\varepsilon}_\omega(\boldsymbol{\omega}) \\ \dot{\tilde{\mathbf{W}}}_\omega = -\frac{1}{2} \eta_\omega \left[ \|\boldsymbol{\alpha}_\omega(\boldsymbol{\omega})\|^2 \tilde{\boldsymbol{\omega}} - \sigma_\omega \hat{\mathbf{W}}_\omega \right] \end{cases} \quad (55)$$

where  $\hat{\mathbf{W}}_\omega = [\hat{W}_{\omega,\phi}, \hat{W}_{\omega,\theta}, \hat{W}_{\omega,\psi}]^T$ ,  $\boldsymbol{\alpha}_\omega(\boldsymbol{\omega}) = [\alpha_{\omega,\phi}, \alpha_{\omega,\theta}, \alpha_{\omega,\psi}]^T$ ,  $\tilde{\mathbf{W}}_\omega = \mathbf{W}_\omega^* - \hat{\mathbf{W}}_\omega$ ,  $\tilde{\boldsymbol{\omega}} = \boldsymbol{\omega} - \hat{\boldsymbol{\omega}}$  and other notations are defined similarly with (8).

Let  $\bar{\boldsymbol{\omega}}(t)$  be the reference command of angular velocity, and its corresponding tracking error is

$$\mathbf{z}_\omega(t) = \boldsymbol{\omega}(t) - \bar{\boldsymbol{\omega}}(t) \quad (56)$$

It follows from (1) that time differential of  $\mathbf{z}_\omega(t)$  can be written as

$$\dot{\mathbf{z}}_\omega(t) = \dot{\boldsymbol{\omega}}(t) - \dot{\bar{\boldsymbol{\omega}}}(t) = \mathbf{f}_\omega(\boldsymbol{\omega}) + \mathbf{g}_\omega \mathbf{u} + \mathbf{d}_\omega - \dot{\bar{\boldsymbol{\omega}}} \quad (57)$$

where  $\mathbf{z}_\omega = [z_{\omega,\phi}, z_{\omega,\theta}, z_{\omega,\psi}]^T$ ,  $\mathbf{g}_\omega = \text{diag}\{\mathbf{g}_{\omega,\phi}, \mathbf{g}_{\omega,\theta}, \mathbf{g}_{\omega,\psi}\}$ .

Afterwards, to avoid unnecessary sampling cost from controller to actuator, based on the event-triggered technology, an adaptive neural controller considering scarce communication bandwidth is synthesized:

$$\begin{cases} \mathcal{G}_a = -\mathbf{g}_a^{-1}(\mathbf{1} + m_{a1}) \left[ \delta_a \tanh\left(\frac{z_{\omega,a} \delta_a}{\xi_a}\right) + \bar{m}_a \tanh\left(\frac{z_{\omega,a} \bar{m}_a}{\xi_a}\right) \right], a = \phi, \theta, \psi \\ \delta_a = k_\omega z_{\omega,a} + \frac{1}{2} \hat{W}_{\omega,a} \|\boldsymbol{\alpha}_{\omega,a}(\boldsymbol{\omega}_a)\|^2 - \dot{\bar{\omega}}_a \end{cases} \quad (58)$$

The triggering event is framed as

$$\begin{aligned} u_a(t) &= \mathcal{G}_a(t_n^a), \forall t \in [t_n^a, t_{n+1}^a), e_{En}^a(t) = \mathcal{G}_a(t) - u_a(t) \\ t_{n+1}^a &= \inf\{t \in R \mid |e_{En}^a(t)| \geq m_{a1} |u_a(t)| + m_{a2}\} \end{aligned} \quad (59)$$

where  $k_\omega$  is a positive control gain.  $\xi_a > 0$ ,  $m_{a1} \in (0, 1]$  and  $m_{a2} > 0$  are design parameters.  $e_{En}^a(t)$  represents triggering error. It is worthwhile mentioning that updating of control signal  $u_a(t)$  is determined by the predesigned triggering condition and from (59),  $u_a(t)$  remains unchanged unless the triggering error surpasses the design threshold. Besides, based on (59), it follows that for each time interval  $t \in [t_n^a, t_{n+1}^a)$ ,  $|\mathcal{G}_a(t) - u_a(t)| \leq m_{a1} |u_a(t)| + m_{a2}$  holds. Thus, there exist time-varying coefficients  $\lambda_{a1}(t), \lambda_{a2}(t)$  fulfilling  $\lambda_{a1}(t_n^a) = 0, \lambda_{a1}(t_{n+1}^a) = \pm 1$  and  $|\lambda_{a1}(t)| \leq 1$ ,  $\lambda_{a2}(t_n^a) = 0, \lambda_{a2}(t_{n+1}^a) = \pm 1$  and  $|\lambda_{a2}(t)| \leq 1$  such that  $\mathcal{G}_a(t) = (1 + \lambda_{a1}(t)m_{a1})u_a(t) + \lambda_{a2}(t)m_{a2}$ . Utilizing the result, we can further obtain  $u_a(t) = (\mathcal{G}_a(t) - \lambda_{a2}(t)m_{a2}) / (1 + \lambda_{a1}(t)m_{a1})$ . The design parameter  $\bar{m}_a$  accounting for stabilizing sampling error in control law (58) satisfies  $\bar{m}_a > \mathbf{g}_{\omega,a} m_{a2} / (1 - m_{a1})$ .

Then, design a Lyapunov function  $V_\omega = \left( \sum_{a \in \{\phi, \theta, \psi\}} z_{\omega,a}^2 \right) / 2$ , and according to (53), (57), (58) together with  $u_a(t) = (\mathcal{G}_a(t) - \lambda_{a2}(t)m_{a2}) / (1 + \lambda_{a1}(t)m_{a1})$ , the time differential can be computed as

$$\begin{aligned}
\dot{V}_\omega &= \sum_{a \in \{\phi, \theta, \psi\}} z_{\omega, a} \dot{z}_{\omega, a} = \sum_{a \in \{\phi, \theta, \psi\}} z_{\omega, a} \left[ f_{\omega, a}(\omega_a) + g_{\omega, a} u_a + d_{\omega, a} - \dot{\tilde{\omega}}_a(t) \right] \\
&= \sum_{a \in \{\phi, \theta, \psi\}} z_{\omega, a} \left[ f_{\omega, a}(\omega_a) + g_{\omega, a} \left( \mathcal{G}_a(t) - \lambda_{a2}(t) m_{a2} \right) / \left( 1 + \lambda_{a1}(t) m_{a1} \right) + d_{\omega, a} - \dot{\tilde{\omega}}_a(t) \right] \\
&= \sum_{a \in \{\phi, \theta, \psi\}} z_{\omega, a} \left[ f_{\omega, a}(\omega_a) + g_{\omega, a} \left( \mathcal{G}_a(t) - \lambda_{a2}(t) m_{a2} \right) / \left( 1 + \lambda_{a1}(t) m_{a1} \right) + d_{\omega, a} + \delta_a - k_\omega z_{\omega, a} - \frac{1}{2} \hat{W}_{\omega, a} \left\| \alpha_{\omega, a}(\omega_a) \right\|^2 \right] \\
&= \sum_{a \in \{\phi, \theta, \psi\}} z_{\omega, a} \left[ g_{\omega, a} \left( \mathcal{G}_a(t) - \lambda_{a2}(t) m_{a2} \right) / \left( 1 + \lambda_{a1}(t) m_{a1} \right) + \delta_a - k_\omega z_{\omega, a} + \frac{1}{2} \tilde{W}_{\omega, a} \left\| \alpha_{\omega, a}(\omega_a) \right\|^2 + \varepsilon_{\omega, a} \right]
\end{aligned} \tag{60}$$

Noting that  $z_{\omega, a} \mathcal{G}_a(t) \leq 0$ ,  $|\lambda_{a1}(t)| \leq 1$  and  $|\lambda_{a2}(t)| \leq 1$ , one has  $z_{\omega, a} \mathcal{G}_a / (1 + \lambda_{a1}(t) m_{a1}) \leq z_{\omega, a} \mathcal{G}_a / (1 + m_{a1})$ ,  $-z_{\omega, a} \lambda_{a2}(t) m_{a2} / (1 + \lambda_{a1}(t) m_{a1}) \leq |z_{\omega, a} m_{a2}| / (1 - m_{a1})$ . Utilizing (58), it follows that

$$\begin{aligned}
\dot{V}_\omega &\leq \sum_{a \in \{\phi, \theta, \psi\}} \left[ z_{\omega, a} g_{\omega, a} \mathcal{G}_a(t) / (1 + m_{a1}) + |z_{\omega, a} g_{\omega, a} m_{a2}| / (1 - m_{a1}) + z_{\omega, a} \left( \delta_a - k_\omega z_{\omega, a} + \frac{1}{2} \tilde{W}_{\omega, a} \left\| \alpha_{\omega, a}(\omega_a) \right\|^2 + \varepsilon_{\omega, a}(\omega_a) \right) \right] \\
&\leq \sum_{a \in \{\phi, \theta, \psi\}} \left[ -z_{\omega, a} \left( \delta_a \tanh\left(\frac{z_{\omega, a} \delta_a}{\xi_a}\right) + \bar{m}_a \tanh\left(\frac{z_{\omega, a} \bar{m}_a}{\xi_a}\right) \right) + |z_{\omega, a} \bar{m}_a| + |z_{\omega, a} \delta_a| + z_{\omega, a} \left( -k_\omega z_{\omega, a} + \frac{1}{2} \tilde{W}_{\omega, a} \left\| \alpha_{\omega, a}(\omega_a) \right\|^2 + \varepsilon_{\omega, a}(\omega_a) \right) \right]
\end{aligned} \tag{61}$$

According to the property of hyperbolic tangent function  $\tanh(\cdot)$ , it follows that

$$0 \leq |\Upsilon| - \Upsilon \tanh\left(\frac{\Upsilon}{\xi}\right) \leq 0.2785 \xi, \quad \Upsilon \in \mathbf{R}, \xi > 0 \tag{62}$$

which further results in

$$\dot{V}_\omega \leq \sum_{a \in \{\phi, \theta, \psi\}} \left( -k_\omega z_{\omega, a}^2 + \frac{1}{2} z_{\omega, a} \tilde{W}_{\omega, a} \left\| \alpha_{\omega, a}(\omega_a) \right\|^2 + z_{\omega, a} \varepsilon_{\omega, a}(\omega_a) + 0.557 \xi_a \right) \tag{63}$$

#### 4. Stability and Zeno phenomena analysis

Define the coupling error  $\tilde{\mathbf{F}} = \mathbf{F} - \mathbf{F}^d$ . Substituting (37), (39), (41) into (35), substituting (43) into (42), substituting (51), (56) into (48), and considering (9), (55) and (57), the following error dynamics involving  $\mathbf{z}_p, \mathbf{z}_v, \mathbf{z}_\theta, \mathbf{z}_\omega, \tilde{\mathbf{v}}, \tilde{\mathbf{W}}_v, \tilde{\omega}, \tilde{\mathbf{W}}_\omega$  can be rewritten as

$$\begin{cases} \dot{\mathbf{z}}_p = -k_p \mathbf{z}_p + \mathbf{B}_p (\boldsymbol{\varsigma}_v + \mathbf{z}_v) \\ \dot{\mathbf{z}}_v = -k_v \mathbf{z}_v + \frac{1}{2} \tilde{\mathbf{W}}_v \left\| \alpha_v(\mathbf{v}) \right\|^2 + \tilde{\mathbf{F}} \\ \dot{\mathbf{z}}_\theta = -k_\theta \mathbf{z}_\theta + \boldsymbol{\varsigma}_\omega + \mathbf{z}_\omega \\ \dot{\mathbf{z}}_\omega = \mathbf{f}_\omega + \mathbf{g}_\omega \mathbf{u} + \mathbf{d}_\omega - \dot{\tilde{\omega}} \end{cases} \tag{64}$$

and

$$\begin{cases} \dot{\tilde{\mathbf{v}}} = \frac{1}{2} \tilde{\mathbf{W}}_v \left\| \alpha_v(\mathbf{v}) \right\|^2 - \kappa_v \tilde{\mathbf{v}} + \boldsymbol{\varepsilon}_v(\mathbf{v}) \\ \dot{\tilde{\mathbf{W}}}_v = -\frac{1}{2} \eta_v \left[ \left\| \alpha_v(\mathbf{v}) \right\|^2 \tilde{\mathbf{v}} - \sigma_v \hat{\mathbf{W}}_v \right] \\ \dot{\tilde{\omega}} = \frac{1}{2} \tilde{\mathbf{W}}_\omega \left\| \alpha_\omega(\boldsymbol{\omega}) \right\|^2 - \kappa_\omega \tilde{\omega} + \boldsymbol{\varepsilon}_\omega(\boldsymbol{\omega}) \\ \dot{\tilde{\mathbf{W}}}_\omega = -\frac{1}{2} \eta_\omega \left[ \left\| \alpha_\omega(\boldsymbol{\omega}) \right\|^2 \tilde{\omega} - \sigma_\omega \hat{\mathbf{W}}_\omega \right] \end{cases} \tag{65}$$

**Theorem 3:** Consider quadrotor dynamics (1), EMLP observer (8), (54), DSC (40), (47), (52) and control signal (58). Under the initial conditions conforming to  $-\bar{\Sigma}_k \chi_k(0) \leq e_{p,k}(0) \leq \bar{\Sigma}_k \chi_k(0)$ ,  $k = x, y, z$ , all the signals in closed-loop system are UUB and the profiles of trajectory tracking errors will be restricted between  $-\bar{\Sigma}_k \chi_k(t)$  and  $\bar{\Sigma}_k \chi_k(t)$  over  $\forall t \in [0, +\infty)$ . Moreover, for any  $n \in \mathbf{Z}^+$ , there exist unknown positive constants  $t_a^* > 0, a = \phi, \theta, \psi$ , such that  $\{t_{n+1}^a - t_n^a\} > t_a^*$ .

**Proof:** Construct an overall Lyapunov function as follows:

$$V = \frac{1}{2} \left\{ \mathbf{z}_p^T \mathbf{z}_p + \mathbf{z}_v^T \mathbf{z}_v + \mathbf{z}_\Theta^T \mathbf{z}_\Theta + \mathbf{z}_\omega^T \mathbf{z}_\omega + \boldsymbol{\varsigma}_v^T \boldsymbol{\varsigma}_v + \boldsymbol{\varsigma}_\Theta^T \boldsymbol{\varsigma}_\Theta + \boldsymbol{\varsigma}_\omega^T \boldsymbol{\varsigma}_\omega + \tilde{\mathbf{v}}^T \tilde{\mathbf{v}} + \tilde{\boldsymbol{\omega}}^T \tilde{\boldsymbol{\omega}} + \eta_v^{-1} \tilde{\mathbf{W}}_v^T \tilde{\mathbf{W}}_v + \eta_\omega^{-1} \tilde{\mathbf{W}}_\omega^T \tilde{\mathbf{W}}_\omega \right\} \quad (66)$$

Recalling the error dynamics (64), (65) and combining (63), the time derivative of (66) can be deduced as

$$\begin{aligned} \dot{V} &\leq \mathbf{z}_p^T \left( -k_p \mathbf{z}_p + \mathbf{B}_p (\boldsymbol{\varsigma}_v + \mathbf{z}_v) \right) + \mathbf{z}_v^T \left( -k_v \mathbf{z}_v + \frac{1}{2} \tilde{\mathbf{W}}_v \|\mathbf{a}_v(\mathbf{v})\|^2 + \tilde{\mathbf{F}} \right) + \mathbf{z}_\Theta^T \left( -k_\Theta \mathbf{z}_\Theta + \boldsymbol{\varsigma}_\omega + \mathbf{z}_\omega \right) + \mathbf{z}_\omega^T \left( -k_\omega \mathbf{z}_\omega + \frac{1}{2} \tilde{\mathbf{W}}_\omega \|\mathbf{a}_\omega(\boldsymbol{\omega})\|^2 + \boldsymbol{\varepsilon}_\omega \right) \\ &+ 0.557 (\xi_\phi + \xi_\theta + \xi_\psi) + \boldsymbol{\varsigma}_v^T \left( -\boldsymbol{\tau}_v^{-1} \boldsymbol{\varsigma}_v + \mathbf{Q}_v(\cdot) \right) + \boldsymbol{\varsigma}_\Theta^T \left( -\boldsymbol{\tau}_\Theta^{-1} \boldsymbol{\varsigma}_\Theta + \mathbf{Q}_\Theta(\cdot) \right) + \boldsymbol{\varsigma}_\omega^T \left( -\boldsymbol{\tau}_\omega^{-1} \boldsymbol{\varsigma}_\omega + \mathbf{Q}_\omega(\cdot) \right) + \tilde{\mathbf{v}}^T \left( \frac{1}{2} \tilde{\mathbf{W}}_v \|\mathbf{a}_v(\mathbf{v})\|^2 - \kappa_v \tilde{\mathbf{v}} + \boldsymbol{\varepsilon}_v \right) \\ &+ \tilde{\boldsymbol{\omega}}^T \left( \frac{1}{2} \tilde{\mathbf{W}}_\omega \|\mathbf{a}_\omega(\boldsymbol{\omega})\|^2 - \kappa_\omega \tilde{\boldsymbol{\omega}} + \boldsymbol{\varepsilon}_\omega \right) - \frac{1}{2} \tilde{\mathbf{W}}_v^T \left( \|\mathbf{a}_v(\mathbf{v})\|^2 \tilde{\mathbf{v}} - \sigma_v \hat{\mathbf{W}}_v \right) - \frac{1}{2} \tilde{\mathbf{W}}_\omega^T \left( \|\mathbf{a}_\omega(\boldsymbol{\omega})\|^2 \tilde{\boldsymbol{\omega}} - \sigma_\omega \hat{\mathbf{W}}_\omega \right) \\ &\leq -k_p \mathbf{z}_p^T \mathbf{z}_p - k_v \mathbf{z}_v^T \mathbf{z}_v - k_\Theta \mathbf{z}_\Theta^T \mathbf{z}_\Theta - k_\omega \mathbf{z}_\omega^T \mathbf{z}_\omega - \lambda_{\min}(\boldsymbol{\tau}_v^{-1}) \boldsymbol{\varsigma}_v^T \boldsymbol{\varsigma}_v - \lambda_{\min}(\boldsymbol{\tau}_\Theta^{-1}) \boldsymbol{\varsigma}_\Theta^T \boldsymbol{\varsigma}_\Theta - \lambda_{\min}(\boldsymbol{\tau}_\omega^{-1}) \boldsymbol{\varsigma}_\omega^T \boldsymbol{\varsigma}_\omega - \kappa_v \tilde{\mathbf{v}}^T \tilde{\mathbf{v}} - \kappa_\omega \tilde{\boldsymbol{\omega}}^T \tilde{\boldsymbol{\omega}} \\ &+ \lambda_{\max}(\mathbf{B}_p) |\mathbf{z}_p^T \boldsymbol{\varsigma}_v| + \lambda_{\max}(\mathbf{B}_p) |\mathbf{z}_p^T \mathbf{z}_v| + \frac{1}{2} |\mathbf{z}_v^T \tilde{\mathbf{W}}_v| \|\mathbf{a}_v(\mathbf{v})\|^2 + |\mathbf{z}_v^T \tilde{\mathbf{F}}| + |\mathbf{z}_\Theta^T \boldsymbol{\varsigma}_\omega| + |\mathbf{z}_\Theta^T \mathbf{z}_\omega| + \frac{1}{2} |\mathbf{z}_\omega^T \tilde{\mathbf{W}}_\omega| \|\mathbf{a}_\omega(\boldsymbol{\omega})\|^2 + |\mathbf{z}_\omega^T \boldsymbol{\varepsilon}_\omega| \\ &+ |\boldsymbol{\varsigma}_v^T \mathbf{Q}_v(\cdot)| + |\boldsymbol{\varsigma}_\Theta^T \mathbf{Q}_\Theta(\cdot)| + |\boldsymbol{\varsigma}_\omega^T \mathbf{Q}_\omega(\cdot)| + |\tilde{\mathbf{v}}^T \boldsymbol{\varepsilon}_v| + |\tilde{\boldsymbol{\omega}}^T \boldsymbol{\varepsilon}_\omega| + \frac{1}{2} \sigma_v |\tilde{\mathbf{W}}_v^T \hat{\mathbf{W}}_v| + \frac{1}{2} \sigma_\omega |\tilde{\mathbf{W}}_\omega^T \hat{\mathbf{W}}_\omega| + 0.557 (\xi_\phi + \xi_\theta + \xi_\psi) \end{aligned} \quad (67)$$

where  $\lambda_{\min}(\cdot)$  and  $\lambda_{\max}(\cdot)$  respectively denotes the minimum and maximum eigenvalue of matrix.

Recalling (1), (44), the coupling error  $\tilde{\mathbf{F}} = [\tilde{F}_x, \tilde{F}_y, \tilde{F}_z]^T$  can be expressed in the following form:

$$\begin{cases} \tilde{F}_x = \frac{u_F}{m} \left[ \left( \cos(\Theta_\psi) \sin(\Theta_\theta) \cos(\Theta_\phi) + \sin(\Theta_\psi) \sin(\Theta_\phi) \right) - \left( \cos(\Theta_\psi^d) \sin(\Theta_\theta^d) \cos(\Theta_\phi^d) + \sin(\Theta_\psi^d) \sin(\Theta_\phi^d) \right) \right] \\ \tilde{F}_y = \frac{u_F}{m} \left[ \left( \sin(\Theta_\psi) \sin(\Theta_\theta) \cos(\Theta_\phi) - \cos(\Theta_\psi) \sin(\Theta_\phi) \right) - \left( \sin(\Theta_\psi^d) \sin(\Theta_\theta^d) \cos(\Theta_\phi^d) - \cos(\Theta_\psi^d) \sin(\Theta_\phi^d) \right) \right] \\ \tilde{F}_z = \frac{u_F}{m} \left[ \cos(\Theta_\theta) \cos(\Theta_\phi) - \cos(\Theta_\theta^d) \cos(\Theta_\phi^d) \right] \end{cases} \quad (68)$$

And referring to [15], the coupling function  $\tilde{\mathbf{F}}$  is Lipschitz in  $\boldsymbol{\Theta} \in \mathbf{R}^3$  and continuous in  $u_F \in \mathbf{R}$ , one has

$$\|\tilde{\mathbf{F}}\| \leq k_F \cdot \|\mathbf{z}_\Theta\|, \forall \boldsymbol{\Theta}, \mathbf{F}^d \in \mathbf{R}^3, \forall u_F \in \mathbf{R} \quad (69)$$

where  $k_F$  is a positive scalar. Thus, (67) can be further rewritten as

$$\begin{aligned} \dot{V} &\leq -k_p \mathbf{z}_p^T \mathbf{z}_p - k_v \mathbf{z}_v^T \mathbf{z}_v - k_\Theta \mathbf{z}_\Theta^T \mathbf{z}_\Theta - k_\omega \mathbf{z}_\omega^T \mathbf{z}_\omega - \lambda_{\min}(\boldsymbol{\tau}_v^{-1}) \boldsymbol{\varsigma}_v^T \boldsymbol{\varsigma}_v - \lambda_{\min}(\boldsymbol{\tau}_\Theta^{-1}) \boldsymbol{\varsigma}_\Theta^T \boldsymbol{\varsigma}_\Theta - \lambda_{\min}(\boldsymbol{\tau}_\omega^{-1}) \boldsymbol{\varsigma}_\omega^T \boldsymbol{\varsigma}_\omega - \kappa_v \tilde{\mathbf{v}}^T \tilde{\mathbf{v}} - \kappa_\omega \tilde{\boldsymbol{\omega}}^T \tilde{\boldsymbol{\omega}} \\ &+ \lambda_{\max}(\mathbf{B}_p) |\mathbf{z}_p^T \boldsymbol{\varsigma}_v| + \lambda_{\max}(\mathbf{B}_p) |\mathbf{z}_p^T \mathbf{z}_v| + \frac{1}{2} |\mathbf{z}_v^T \tilde{\mathbf{W}}_v| \|\mathbf{a}_v(\mathbf{v})\|^2 + k_F |\mathbf{z}_v^T \mathbf{z}_\Theta| + |\mathbf{z}_\Theta^T \boldsymbol{\varsigma}_\omega| + |\mathbf{z}_\Theta^T \mathbf{z}_\omega| + \frac{1}{2} |\mathbf{z}_\omega^T \tilde{\mathbf{W}}_\omega| \|\mathbf{a}_\omega(\boldsymbol{\omega})\|^2 + |\boldsymbol{\varsigma}_v^T \mathbf{Q}_v(\cdot)| \\ &+ |\boldsymbol{\varsigma}_\Theta^T \mathbf{Q}_\Theta(\cdot)| + |\boldsymbol{\varsigma}_\omega^T \mathbf{Q}_\omega(\cdot)| + |\tilde{\mathbf{v}}^T \boldsymbol{\varepsilon}_v| + |\tilde{\boldsymbol{\omega}}^T \boldsymbol{\varepsilon}_\omega| + \frac{1}{2} \sigma_v |\tilde{\mathbf{W}}_v^T \hat{\mathbf{W}}_v| + \frac{1}{2} \sigma_\omega |\tilde{\mathbf{W}}_\omega^T \hat{\mathbf{W}}_\omega| + 0.557 (\xi_\phi + \xi_\theta + \xi_\psi) \end{aligned} \quad (70)$$

Define the set  $\Omega_1 = \left\{ \mathbf{z}_p^T \mathbf{z}_p + \mathbf{z}_v^T \mathbf{z}_v + \mathbf{z}_\Theta^T \mathbf{z}_\Theta + \mathbf{z}_\omega^T \mathbf{z}_\omega + \boldsymbol{\varsigma}_v^T \boldsymbol{\varsigma}_v + \boldsymbol{\varsigma}_\Theta^T \boldsymbol{\varsigma}_\Theta + \boldsymbol{\varsigma}_\omega^T \boldsymbol{\varsigma}_\omega + \tilde{\mathbf{v}}^T \tilde{\mathbf{v}} + \tilde{\boldsymbol{\omega}}^T \tilde{\boldsymbol{\omega}} + \eta_v^{-1} \tilde{\mathbf{W}}_v^T \tilde{\mathbf{W}}_v + \eta_\omega^{-1} \tilde{\mathbf{W}}_\omega^T \tilde{\mathbf{W}}_\omega \leq 2\varpi \right\}$ ,

where  $\varpi$  is a positive constant. Combining with Assumption 1, we can derive that the vectors  $\mathbf{Q}_v(\cdot), \mathbf{Q}_\Theta(\cdot), \mathbf{Q}_\omega(\cdot)$  given in (40), (47) and (52) are within the compact set  $\Omega_0 \times \Omega_1$ , i.e.,  $\|\mathbf{Q}_v(\cdot)\|, \|\mathbf{Q}_\Theta(\cdot)\|, \|\mathbf{Q}_\omega(\cdot)\|$  satisfy  $\|\mathbf{Q}_v(\cdot)\| \leq Q_v^*$ ,

$\|\mathbf{Q}_\Theta(\cdot)\| \leq Q_\Theta^*, \|\mathbf{Q}_\omega(\cdot)\| \leq Q_\omega^*$  with  $Q_v^*, Q_\Theta^*, Q_\omega^*$  being positive constants. Then, resorting to Young's inequality, it yields

$$\begin{aligned} |\mathbf{z}_p^T \boldsymbol{\varsigma}_v| &\leq \frac{\lambda_1^*}{2} \|\mathbf{z}_p\|^2 + \frac{\|\boldsymbol{\varsigma}_v\|^2}{2\lambda_1^*}, |\mathbf{z}_p^T \mathbf{z}_v| \leq \frac{\lambda_2^*}{2} \|\mathbf{z}_p\|^2 + \frac{\|\mathbf{z}_v\|^2}{2\lambda_2^*}, \frac{1}{2} |\mathbf{z}_v^T \tilde{\mathbf{W}}_v| \|\mathbf{a}_v(\mathbf{v})\|^2 \leq \frac{\bar{\alpha}_v^4 \cdot \|\mathbf{z}_v\|^2}{4\zeta_v^*} + \frac{\zeta_v^* \|\tilde{\mathbf{W}}_v\|^2}{4}, |\mathbf{z}_v^T \mathbf{z}_\Theta| \leq \frac{\|\mathbf{z}_v\|^2}{2} + \frac{\|\mathbf{z}_\Theta\|^2}{2}, |\mathbf{z}_\Theta^T \boldsymbol{\varsigma}_\omega| \leq \frac{\|\mathbf{z}_\Theta\|^2}{2} + \frac{\|\boldsymbol{\varsigma}_\omega\|^2}{2}, \\ |\mathbf{z}_\Theta^T \mathbf{z}_\omega| &\leq \frac{\|\mathbf{z}_\Theta\|^2}{2} + \frac{\|\mathbf{z}_\omega\|^2}{2}, \frac{1}{2} |\mathbf{z}_\omega^T \tilde{\mathbf{W}}_\omega| \|\mathbf{a}_\omega(\boldsymbol{\omega})\|^2 \leq \frac{\bar{\alpha}_\omega^4 \cdot \|\mathbf{z}_\omega\|^2}{4\zeta_\omega^*} + \frac{\zeta_\omega^* \|\tilde{\mathbf{W}}_\omega\|^2}{4}, |\mathbf{z}_\omega^T \boldsymbol{\varepsilon}_\omega| \leq \frac{\|\mathbf{z}_\omega\|^2}{2} + \frac{\bar{\varepsilon}_\omega^2}{2}, |\boldsymbol{\varsigma}_v^T \mathbf{Q}_v(\cdot)| \leq \frac{\|\boldsymbol{\varsigma}_v\|^2}{2} + \frac{Q_v^{*2}}{2}, |\boldsymbol{\varsigma}_\Theta^T \mathbf{Q}_\Theta(\cdot)| \leq \frac{\|\boldsymbol{\varsigma}_\Theta\|^2}{2} + \frac{Q_\Theta^{*2}}{2}, \\ |\boldsymbol{\varsigma}_\omega^T \mathbf{Q}_\omega(\cdot)| &\leq \frac{\|\boldsymbol{\varsigma}_\omega\|^2}{2} + \frac{Q_\omega^{*2}}{2}, |\tilde{\mathbf{v}}^T \boldsymbol{\varepsilon}_v| \leq \frac{\|\tilde{\mathbf{v}}\|^2}{2} + \frac{\bar{\varepsilon}_v^2}{2}, |\tilde{\boldsymbol{\omega}}^T \boldsymbol{\varepsilon}_\omega| \leq \frac{\|\tilde{\boldsymbol{\omega}}\|^2}{2} + \frac{\bar{\varepsilon}_\omega^2}{2}, |\tilde{\mathbf{W}}_v^T \hat{\mathbf{W}}_v| \leq \frac{\|\tilde{\mathbf{W}}_v\|^2}{2} - \frac{\|\hat{\mathbf{W}}_v\|^2}{2}, |\tilde{\mathbf{W}}_\omega^T \hat{\mathbf{W}}_\omega| \leq \frac{\|\tilde{\mathbf{W}}_\omega\|^2}{2} - \frac{\|\hat{\mathbf{W}}_\omega\|^2}{2} \end{aligned} \quad (71)$$

Substituting (71) into (67), one gets

$$\begin{aligned}
\dot{V} \leq & -(k_p - \frac{\lambda_1^* + \lambda_2^*}{2} \lambda_{\max}(\mathbf{B}_p)) \|\mathbf{z}_p\|^2 - (k_v - \frac{\lambda_{\max}(\mathbf{B}_p)}{2\lambda_2^*} - \frac{\bar{\alpha}_v^4}{4\zeta_v^*} - \frac{k_F}{2}) \|\mathbf{z}_v\|^2 - (k_\theta - \frac{k_F}{2} - 1) \|\mathbf{z}_\theta\|^2 - (k_\omega - 1 - \frac{\bar{\alpha}_\omega^4}{4\zeta_\omega^*}) \|\mathbf{z}_\omega\|^2 \\
& - (\lambda_{\min}(\boldsymbol{\tau}_v^{-1}) - \frac{1}{2} - \frac{\lambda_{\max}(\mathbf{B}_p)}{2\lambda_1^*}) \|\boldsymbol{\varsigma}_v\|^2 - (\lambda_{\min}(\boldsymbol{\tau}_\theta^{-1}) - \frac{1}{2}) \|\boldsymbol{\varsigma}_\theta\|^2 - (\lambda_{\min}(\boldsymbol{\tau}_\omega^{-1}) - 1) \|\boldsymbol{\varsigma}_\omega\|^2 - (\kappa_v - \frac{1}{2}) \|\tilde{\mathbf{v}}\|^2 - (\kappa_\omega - \frac{1}{2}) \|\tilde{\boldsymbol{\omega}}\|^2 - (\frac{\sigma_v}{4} \\
& - \frac{\zeta_v^*}{4}) \|\tilde{\mathbf{W}}_v\|^2 + (\frac{\sigma_\omega}{4} - \frac{\zeta_\omega^*}{4}) \|\tilde{\mathbf{W}}_\omega\|^2 + \frac{Q_v^{*2}}{2} + \frac{Q_\theta^{*2}}{2} + \frac{Q_\omega^{*2}}{2} + \frac{\bar{\varepsilon}_v^2}{2} + \bar{\varepsilon}_\omega^2 + \frac{\sigma_v \|\mathbf{W}_v^*\|^2}{4} + \frac{\sigma_\omega \|\mathbf{W}_\omega^*\|^2}{4} + 0.557(\xi_\phi + \xi_\theta + \xi_\psi)
\end{aligned} \quad (72)$$

Following (72), one has

$$\dot{V} \leq -\mu_s V + \beta_s \quad (73)$$

where  $\beta_s = Q_v^{*2}/2 + Q_\theta^{*2}/2 + Q_\omega^{*2}/2 + \bar{\varepsilon}_v^2/2 + \bar{\varepsilon}_\omega^2 + \sigma_v \|\mathbf{W}_v^*\|^2/4 + \sigma_\omega \|\mathbf{W}_\omega^*\|^2/4 + 0.557(\xi_\phi + \xi_\theta + \xi_\psi)$  and  $\mu_s = \min\{2\mu_1, 2\mu_2, 2\mu_3, 2\mu_4, 2\mu_5, 2\mu_6, 2\mu_7, 2\mu_8, 2\mu_9, 2\mu_{10}, 2\eta_v, \mu_{11}\} > 0$ , whose components fulfill

$$\begin{aligned}
\mu_1 &= k_p - (\lambda_1^* + \lambda_2^*) \lambda_{\max}(\mathbf{B}_p) / 2 > 0, \mu_2 = k_v - \lambda_{\max}(\mathbf{B}_p) / 2\lambda_2^* - \bar{\alpha}_v^4 / 4\zeta_v^* - k_F / 2 > 0, \mu_3 = k_\theta - k_F / 2 - 1 > 0, \\
\mu_4 &= k_\omega - 1 - \bar{\alpha}_\omega^4 / 4\zeta_\omega^* > 0, \mu_5 = \lambda_{\min}(\boldsymbol{\tau}_v^{-1}) - 1/2 - \lambda_{\max}(\mathbf{B}_p) / 2\lambda_1^* > 0, \mu_6 = \lambda_{\min}(\boldsymbol{\tau}_\theta^{-1}) - 1/2 > 0, \mu_7 = \lambda_{\min}(\boldsymbol{\tau}_\omega^{-1}) \\
&- 1 > 0, \mu_8 = \kappa_v - 1/2 > 0, \mu_9 = \kappa_\omega - 1/2 > 0, \mu_{10} = \sigma_v / 4 - \zeta_v^* / 4 > 0, \mu_{11} = \sigma_\omega / 4 - \zeta_\omega^* / 4 > 0
\end{aligned} \quad (74)$$

Since  $\mu_s \geq \beta_s / \varpi$  on  $V = \varpi$  can lead to  $\dot{V} \leq 0$  from (73), we have  $V(t) \leq \varpi, \forall t \geq 0$  for  $V(0) \leq \varpi$ . Solving (73) results in

$$0 \leq V \leq \frac{\beta_s}{\mu_s} (1 - e^{-\mu_s t}) + V(0) e^{-\mu_s t} \quad (75)$$

Evidently, the boundedness of error dynamics  $\mathbf{z}_p, \mathbf{z}_v, \mathbf{z}_\theta, \mathbf{z}_\omega, \boldsymbol{\varsigma}_v, \boldsymbol{\varsigma}_\theta, \boldsymbol{\varsigma}_\omega, \tilde{\mathbf{v}}, \tilde{\mathbf{W}}_v, \tilde{\boldsymbol{\omega}}, \tilde{\mathbf{W}}_\omega$  can be ensured and as  $t \rightarrow \infty$ , one has

$$\begin{aligned}
\|\mathbf{z}_p\| &\leq \sqrt{2\beta_s / \mu_s}, \|\mathbf{z}_v\| \leq \sqrt{2\beta_s / \mu_s}, \|\mathbf{z}_\theta\| \leq \sqrt{2\beta_s / \mu_s}, \|\mathbf{z}_\omega\| \leq \sqrt{2\beta_s / \mu_s}, \\
\|\boldsymbol{\varsigma}_v\| &\leq \sqrt{2\beta_s / \mu_s}, \|\boldsymbol{\varsigma}_\theta\| \leq \sqrt{2\beta_s / \mu_s}, \|\boldsymbol{\varsigma}_\omega\| \leq \sqrt{2\beta_s / \mu_s}, \|\tilde{\mathbf{v}}\| \leq \sqrt{2\beta_s / \mu_s}, \\
\|\tilde{\mathbf{W}}_v\| &\leq \sqrt{2\beta_s / \mu_s}, \|\tilde{\boldsymbol{\omega}}\| \leq \sqrt{2\beta_s / \mu_s}, \|\tilde{\mathbf{W}}_\omega\| \leq \sqrt{2\beta_s / \mu_s}
\end{aligned} \quad (76)$$

It can be obtained from (76) that all signals in closed-loop system can realize UUB results and combining with Lemma 2, we can deduce that if the initial conditions  $-\bar{\Sigma}_k \chi_k(0) \leq e_{p,k}(0) \leq \bar{\Sigma}_k \chi_k(0), k = x, y, z$  are satisfied, trajectory tracking errors are constrained within the predefined envelopes. Thus, time derivatives of control inputs are bounded, i.e.,  $|\dot{u}_a| \leq \tilde{\lambda}_a$  with  $\tilde{\lambda}_a$  being a positive constant. Define the maximum triggering error as  $\bar{e}_{En}^a = m_{a1} |\mathcal{G}_a(t)| + m_{a2}$  by making use of the event-triggered condition (59), note that for every inter-execution interval  $(t_n^a, t_{n+1}^a]$ , we can derive that  $e_{En}^a(t_n^a) = 0$  and  $e_{En}^a(t_{n+1}^a) = \bar{e}_{En}^a$ , which leads to  $\{t_{n+1}^a - t_n^a\} \geq t^* \triangleq \bar{e}_{En}^a / \tilde{\lambda}_a$ . Therefore, Zeno phenomena for quadrotors can be removed.

The proof of Theorem 3 is completed.

**Remark 6:** To facilitate simulation implementation of the proposed algorithms, some guidelines for turning parameters can be summarized here:

- 1) From (76), we can know that the residual sets will get smaller as control gains  $k_p, k_v, k_\theta, k_\omega$  increases, which leads to a high tracking accuracy and fast convergence rate. Nevertheless, if the selection of control gain is overlarge, oscillation phenomenon will inevitably appear in control inputs, causing a threat for normal operation of quadrotors.
- 2) For APPC, an arbitrarily small prescribed time can be theoretically achieved by turning design parameter  $T$ . However, control inputs may exceed the allowable range of actuator, resulting in actuator saturation. Hence,  $T$  should be appropriately chosen.
- 3) For the presented EMLP observer, the selections of observer bandwidths  $\kappa_v, \kappa_\omega$  should be chosen sufficiently larger than control gains  $k_v, k_\omega$ . Generally speaking, in order to implement the time-scale separation between control and learning loops, observer bandwidths should be designed as 2-3 times larger than control gains. In addition, adaptive gains  $\eta_v, \eta_\omega$  should be reasonably high enough to accomplish high-precision identifications for unavailable uncertainties.

## 5. Simulation results

In the section, extensive numerical simulations are performed to demonstrate the effectiveness of proposed algorithms under MATLAB/SIMULINK environment, while the related physical parameters for quadrotors are borrowed from [46] including  $m = 2kg$ ,  $g = 9.8m/s^2$ ,  $c = 0.05$ ,  $l = 0.4m$ ,  $\mathbf{J} = [0.16, 0.16, 0.32]^T kgm^2$ . Setting initial states as  $\mathbf{p}(0) = [-3.5, 3.5, 1]^T m$  and  $\mathbf{\Theta}(0) = [0, 0, 0.2]^T deg$ . Next, to verify the robustness of the designed controller, the damping matrices are devised as  $\mathbf{\Pi}_v = diag\{0.01, 0.01, 0.01\} Nms^2$ ,  $\mathbf{\Pi}_\omega = diag\{0.012, 0.012, 0.012\} Nms^2$ , and uncertainties of aerodynamic coefficients are taken as -30% of the nominal values, and external disturbances acting on quadrotors are designed as  $\mathbf{d}_v = [2(\sin(t) + \sin(0.5t) - \cos(0.8t)), 2(\cos(t) + \sin(0.5t) - \cos(0.8t)), 2\sin(1.5t)]^T$ ,  $\mathbf{d}_\omega = [0.2(\sin(t) + \sin(0.5t)), 0.2(\cos(0.5t) - \cos(0.8t)), 0.2\sin(t)\sin(0.5t)]^T$ . Besides, parameters of the presented controller are listed in Table.1 and reference command to be tracked is given as

$$\mathbf{p}^d = \begin{cases} [0, 0, 9(1 - e^{-0.3t})]^T, & t \leq 9 \\ [10(1 - \cos(2\pi(t-9)/23)), 5\sin(4\pi(t-9)/23), 9(1 - e^{-0.3t})]^T, & t > 9 \end{cases} \quad (77)$$

Table.1 Parameters for proposed algorithm

Sections	Values
APPC	$T = 5, \bar{h} = 0.4, \bar{s}_x = \bar{s}_y = \bar{s}_z = 1, \underline{s}_x = \underline{s}_y = \underline{s}_z = 0.8.$
EMLP observer	$\kappa_v = 6.5, \kappa_\omega = 21, \eta_v = 15, \eta_\omega = 50, \sigma_v = 0.06, \sigma_\omega = 0.02.$
DSC	$\boldsymbol{\tau}_v = \boldsymbol{\tau}_\omega = \boldsymbol{\tau}_\omega = diag\{0.001, 0.001, 0.001\}.$
Event-triggered controller	$k_p = 1.5, k_v = 3, k_\theta = 4, k_\omega = 8, \xi_\phi = \xi_\theta = \xi_\psi = 2000, \bar{m}_\phi = \bar{m}_\theta = \bar{m}_\psi = 100.$ $m_{\phi 1} = 0.2, m_{\theta 1} = 0.2, m_{\psi 1} = 0.2, m_{\phi 2} = 0.05, m_{\theta 2} = 0.05, m_{\psi 2} = 0.1,$

### A. Simulation verification of the derived results

To confirm the effectiveness of presented control method in realizing a desirable tracking performance, simulations are executed and relevant results are illustrated in Figs.5-9. As displayed in Fig.5, the desired 8-shaped trajectory can be perfectly tracked with nonzero initial tracking errors. Fig.6 gives response curves of trajectory tracking errors, where we can intuitively see that both transient and steady-state performances for quadrotors can strictly fulfill the prescribed specification, meanwhile all prescribed boundaries converge to the predetermined steady-state values within an appointed time. From Fig.7, position and attitude responses can smoothly follow the reference signals, regardless of the existence of unavailable external disturbances and unknown system dynamics. As depicted in Fig.8, it is evident that by applying event-triggered method to quadrotor systems, sampling times for control inputs can be remarkably reduced, greatly releasing transmission burden in controller-to-actuator communication channels. Fig.9 shows that lumped disturbances can be precisely estimated by EMLP observer.

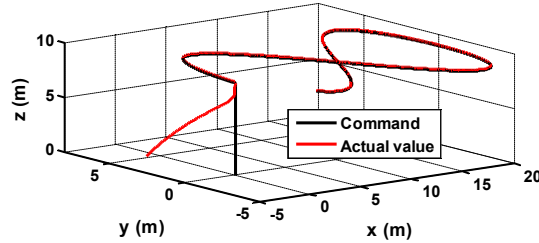


Fig.5 Eight-shaped trajectory tracking result

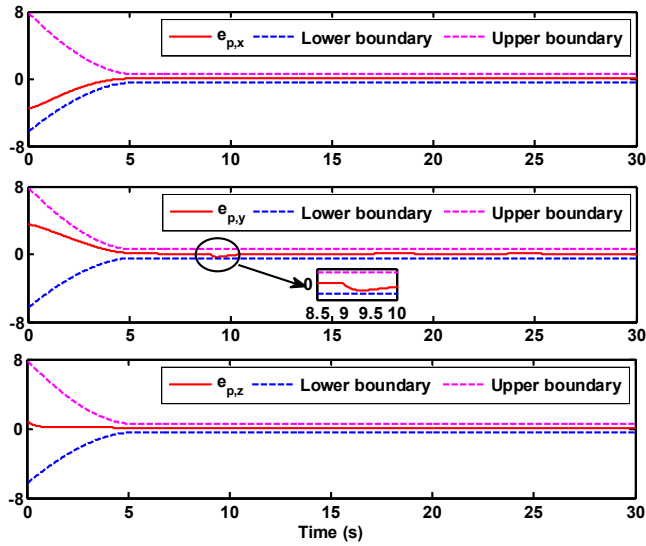


Fig.6 Convergence performance of trajectory tracking errors

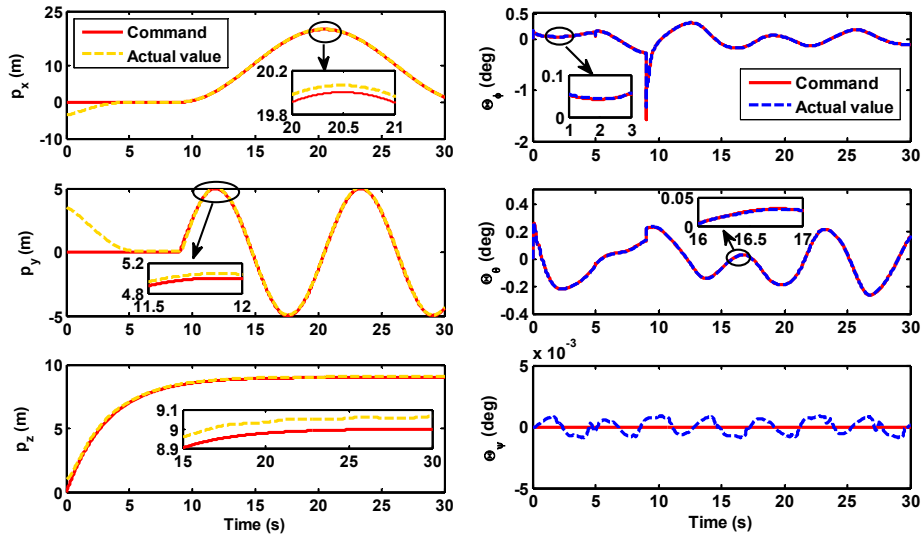


Fig.7 Response curves of position and attitude

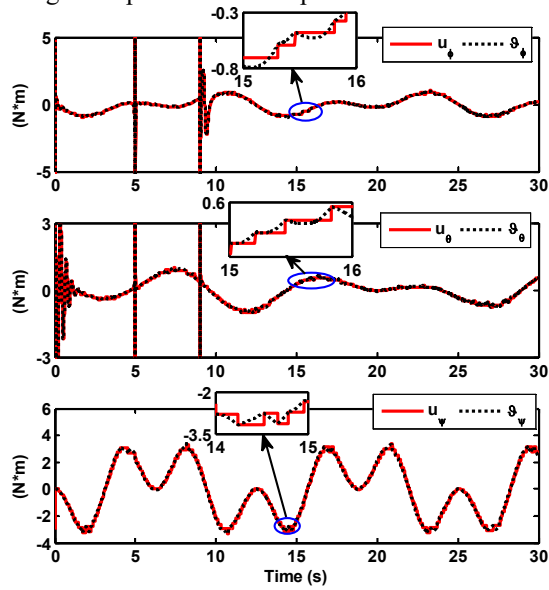


Fig.8 Control inputs

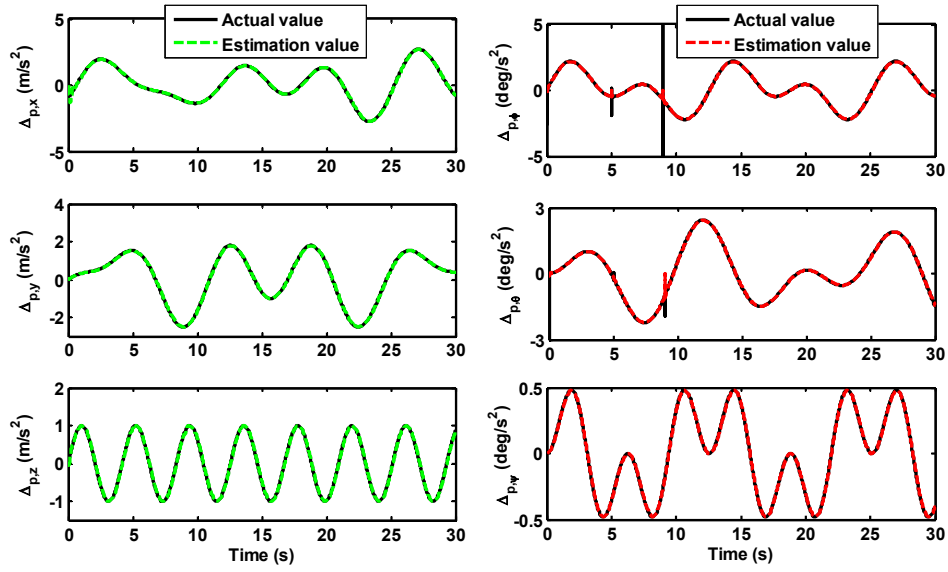


Fig.9 Estimates of lumped disturbances in translational and rotational loops

In order to further highlight the superiority of the proposed controller, we make a simulation comparison with the work [52], and assuring comparison fairness, the related control parameters are delicately adjusted via trial and error, such that nearly the same steady-state tracking precision can be attained. Numerical simulations are illustrated in Fig.10 and corresponding quantitative results, in terms of prescribed time, convergence time, updating times and standard deviation of tracking error, are given in Table 2.

From Fig.10, both of two control methods can restrict the trajectory tracking errors to prescribed boundaries, but an obvious fact is that performance boundaries of PPC cannot precisely reach the pre-given final value within a finite time, which naturally results in a prolong transient error convergence process. However, the proposed APPC with an appointed time arrival ability is more superior in guaranteeing transient performances with a finite convergence time, which is only related to the parameter of behavior bound, irrespective of other controller gains or system initial states. And in comparison to the scheme in Ref. [52], our proposed scheme uses a relative threshold condition to schedule the sampling time instant sequence, greatly decreasing the transmission data in controller to actuator channel, which allows for a relaxed transmission burden and a reduced sampling cost. Furthermore, as can be seen from Table 2, our scheme can exhibit a shorter error convergence time, and reduced amount of sampling times under the premise of the same steady-state tracking errors compared to Ref. [52], thus the proposed control strategy is more suitable to implement in a hardware resource-aware quadrotor system suffering from various disturbances.

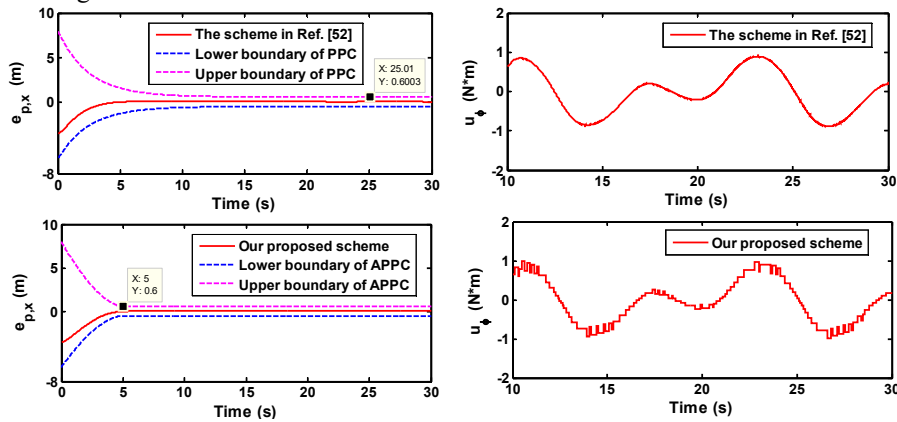


Fig.10 Comparison result with control scheme in Ref. [52]

Table.2 Quantitative comparison with control scheme in Ref. [52]

Index	Our proposed scheme	The scheme in Ref. [52]
-------	---------------------	-------------------------

Prescribed time <sup>a</sup>	5s	$+\infty$
Convergence time <sup>b</sup>	4.35s	5.52s
Updating times of $u_\phi$	332	30000
Standard deviation of $e_{p,x}$	0.0049	0.0048

- a. Prescribed time corresponds to the time instant when performance boundary firstly reaches to the specified final value.  
b. Convergence time refers to the moment that trajectory tracking error firstly enters inside the range  $[-0.3, 0.3]$ .

## B. Performance verification and comparative studies

### Case 1. Comparative studies among RBFNN [40], MLP [50] and EMLP observer

In the subsection, it should be pointed out that RBFNN and MLP have almost the same estimation capability due to employment of tracking errors to update NN weight. Consequently, the involved simulation only provides comparative results between MLP and EMLP observer. Here, we take yaw channel for instance to demonstrate the efficacy of disturbances estimation performance for comparative methods. And to ensure the fairness of comparison, the same controller parameters and adaptive gains for quadrotors are selected.

Firstly, to compare identification capability of MLP and EMLP observer against a low-frequency disturbance, we modify external disturbance as  $d_\psi = 0.2\sin(0.5t)\sin(0.25t)$ . As seen from Fig.11, when the adaptive gain is chosen as  $\eta_\omega = 5$ , both MLP and EMLP observer can achieve precise estimates for low frequency disturbances, but it can be observed that results of EMLP observer is a bit smoother than that of MLP observer.

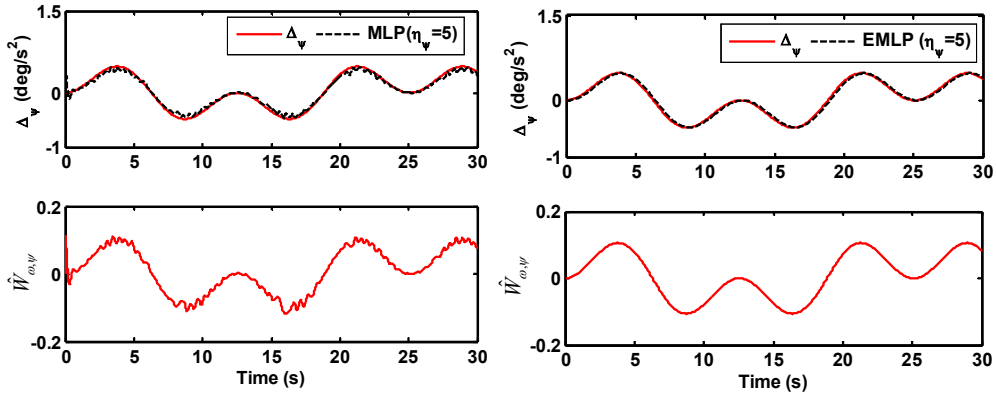


Fig.11 Profiles comparison between MLP [50] and EMLP observer under a low-frequency disturbance

Furthermore, to compare identification capability of MLP and EMLP observer for a high-frequency disturbance, a relatively fast time-varying external disturbance is considered as  $d_\psi = 0.2\sin(8t)\sin(4t)$ . As depicted in Fig.12, as the adaptive gain increases, although the steady-state estimation ability tends to be better for MLP, the transient behaviors aggravate with several oscillations. While for EMLP observer, a smooth and rapid estimation can be obtained and high-frequency vibrations are not incurred. Evidently, in contrast of MLP, EMLP observer not only relieves the limitations on maximum learning rate, but also permits a wider range of adaptive gain, which is more suitable for handling fast time-varying uncertainties. Besides, we can discern from Fig.12 that under MLP, owing to the negative impact of identification results, severe oscillations inevitably appear in profiles of control inputs.

For a clearer contrast, estimation performance is quantified in terms of chattering degree, computational burden and steady-state estimation property. Through the data recorded in Table.3, it can be found that compared with MLP and RBFNN, EMLP observer can provide the least oscillations involved in NN weights especially when control system suffers from high-frequency disturbances. Meanwhile, as far as computational burden is concerned, different from the available RBFNN, both MLP and EMLP observer can avoid the tedious learning process, and the computation time of EMLP observer is slightly longer than MLP due to the construction of state observer, which is acceptable. Obviously, the above simulation results reveal that the proposed EMLP observer is superior in decreasing transient oscillations and computational burden, which conforms to Theorem 1 and previous conclusions.

Table.3 Performance comparison among EMLP observer, MLP [50] and RBFNN [40]

Condition	Index	EMLP	MLP [50]	RBFNN [40]
Low-frequency disturbance	Chattering degree <sup>c</sup>	<b>0.002</b>	0.012	0.014
	Computational burden <sup>d</sup>	<b>14.5%</b>	9.8%	35.1%
	Steady-state estimation accuracy	0.0275	0.0387	0.0326
High-frequency disturbance	Chattering degree <sup>c</sup>	<b>0.009</b>	0.789	0.780
	Computational burden <sup>d</sup>	<b>13.9%</b>	10.2%	37.4%
	Steady-state estimation accuracy	0.0075	0.0083	0.0091

c. Computational burden denotes the ratio of accumulated adaptive updating time to the total simulation time.

d. Chattering degree  $L_c$  is calculated in the following form:

$$L_c = \sqrt{\frac{\sum_{n=1}^N |\hat{W}_\psi(n\Delta T) - \hat{W}_\psi((n-1)\Delta T)|^2}{\sum_{n=1}^N |\hat{W}_\psi(n)|^2}} \quad (78)$$

where  $\Delta T$  denotes the time interval and  $N$  is the number of recorded digital signals.

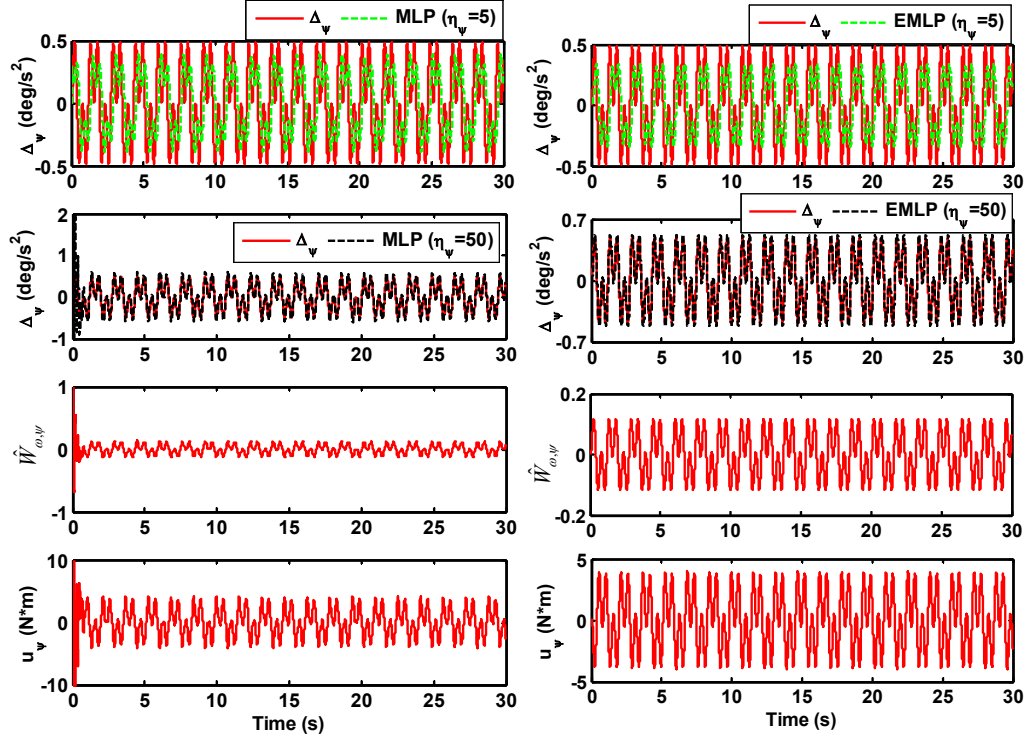


Fig.12 Profiles comparison between MLP [50] and EMLP observer under a high-frequency disturbance

### Case 2. Comparative studies between relative and fixed [49] event-triggered methods

In the subsection, taking control input of yaw channel for instance, we conduct a comparison between the presented event-triggered approach based on a relative threshold and the current fixed threshold event-triggered scheme [49]. Simulation results, in terms of update times of control inputs along with trajectory tracking precision, are shown in Fig.13. Apparently, trajectory tracking errors can converge to a small neighborhood of origin for both methods, and signal updating times using the relative event-triggered method is less than that of fixed event-triggered approach, particularly when the magnitude of control input becomes larger. The fact can be attributed to the designed triggering conditions correlated with control inputs, and it is worth noting that by setting a minimum triggering interval, the proposed event-triggered method eliminates Zeno behavior and avoids dead zone problem. To further evaluate the advantages of the presented controller in

reducing information exchange, a mass of data is collected in Table.4, from which we can conclude that the presented event-triggered controller is more energy-efficient than event-triggered controller based on a fixed threshold with nearly the same tracking accuracy.

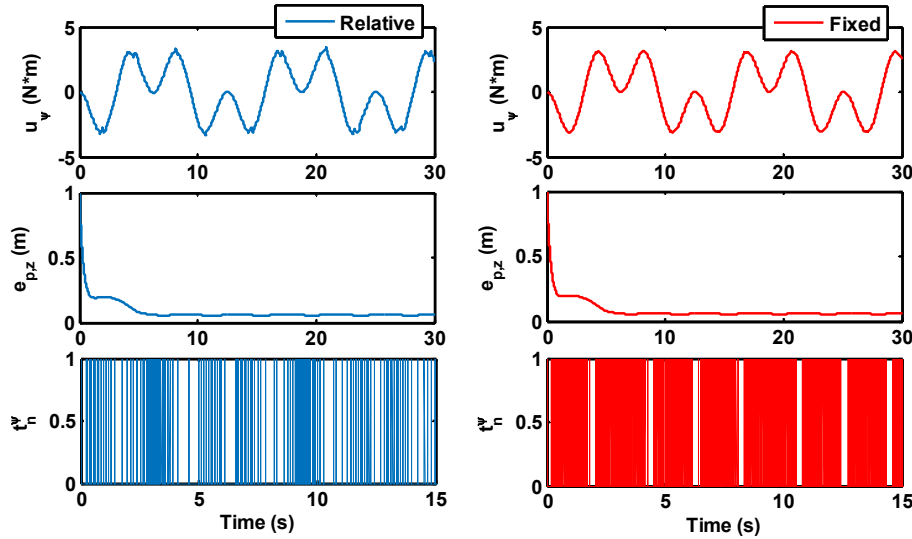


Fig.13 Performance comparison between relative and fixed [49] event-triggered methods

Table.4 Performance comparison among relative event-triggered, fixed event-triggered [49]and continuous-time [46] methods

Index	Relative	Fixed [49]	Continuous-time [46]
Updating times of $u_\psi$	<b>214</b>	1155	30000
Standard deviation of $e_{p,z}$	0.0043	0.0042	0.0042

### Case 3. Performance verification for APPC

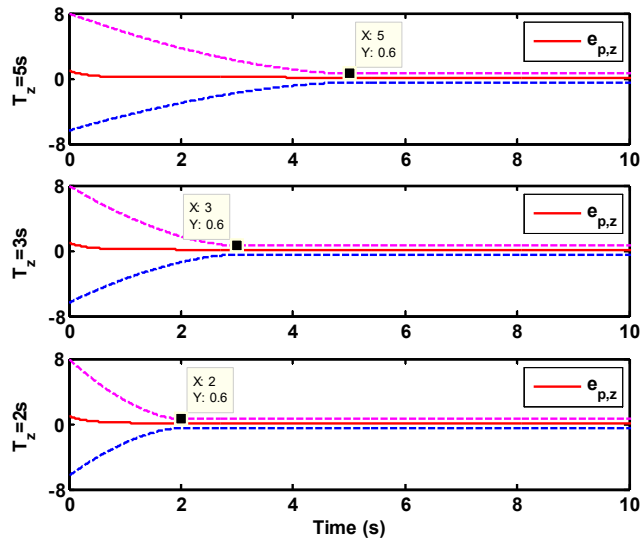


Fig.14 Response curves of  $e_{p,z}$  under different prescribed times

To certify the efficacy of applied APPC in implementing performance boundaries convergence with appointed time constraints, we make simulation verification under different prescribed times. It can be observed from Fig.14 that, by virtue of APPC, boundaries of trajectory tracking errors are restricted to predesigned values and different settling times can be easily regulated using designed parameters  $T = 2s, 3s, 5s$ , which not only clearly illustrates the appointed time convergence ability of the proposed controller, but also provides an effective option for practical engineering employment. Moreover, the objective of Table.5 is to test the convergence property of APPC with different prescribed times. It is shown

that the error convergence time is less than the corresponding prescribed time, exhibiting that the settling time of quadrotors using APPC is free from controller parameters and initial states.

Table.5 Comparison of convergence performance under different prescribed times

Prescribed time	$T = 2s$	$T = 3s$	$T = 5s$
Convergence time of $e_{p,z}$	1.93s	2.78s	4.20s

**Remark 7:** The note is added to describe the procedure for experimental verification of proposed control method. List of equipment has been given to set up a quadrotor experimental platform that can validate and test the presented algorithms. Fig. 15 illustrates system structure diagram of experiment, which consists of motion capture system, ground control system and Pixhawk flight system. Herein, a motion capture system comprising of four synchronized optical cameras attached to ground control system may resort to **Links-GCS manufactured by Beijing Links Co., Ltd.**, which are employed to provide accurate position and velocity measurement of quadrotors, while the attitude and angular rate of quadrotors can be estimated with the aid of complementary filters based on a low cost onboard inertial measurement unit (IMU). Furthermore, a ground control system is responsible for sending user-defined command and data collection during the experiment. And the Pixhawk flight system is used to online execute the suggested control algorithms with a sampling period being 250ms. It is worthwhile stressing that an electrical fan is introduced to supply external wind disturbances to justify the robustness of proposed method.

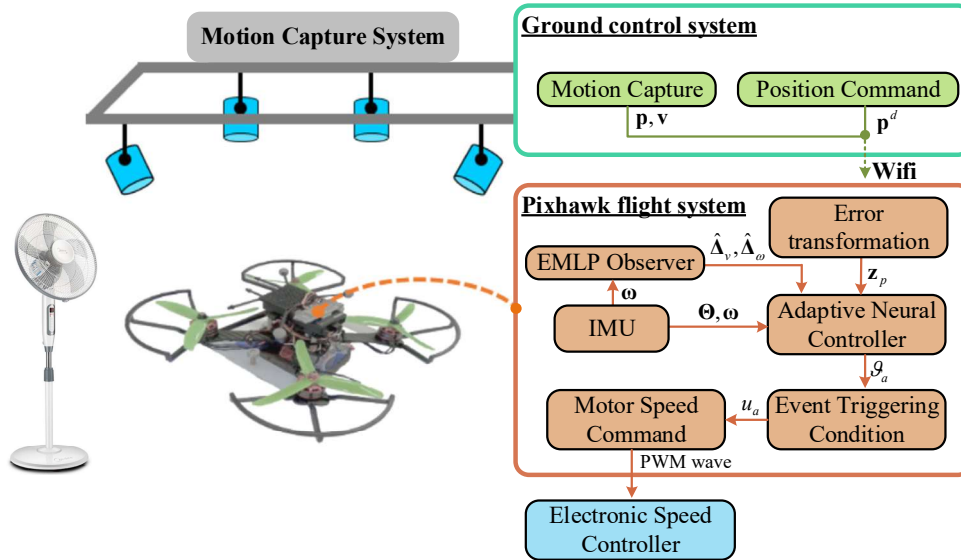


Fig.15 System structure diagram of experiment

## 6. Conclusion

In the paper, a prescribed chattering reduction control for quadrotors using aperiodic signal updating is investigated. Inspired by MLP, an EMLP observer is presented to simultaneously reduce computational burden and transient oscillations inherent in the existing RBFNN with a large adaptive gain. In addition, to ensure a preselected fast convergence time, APPC with a piecewise and continuous finite-time behavior function is developed, such that guaranteed properties in terms of convergence rate, overshoot and steady-state accuracy can be realized. Furthermore, a relative event-triggered robust control law is constructed to save limited communication resources without affecting control precision.

In the near future, we will devote to dealing with an event-triggered output-based control for quadrotors and its related experimental application and pursuing a rigorous time-scale separation theoretical analysis for the involved EMLP and controller.

## Funding

This research has been supported in part by National Natural Science Foundation of China under grant 61803348.

## References

- [1] Z.Y. Lv, Y.H. Wu, W. Rui, Nonlinear motion control for a quadrotor transporting a cable-suspended payload, *IEEE Transactions on Vehicular Technology*, 69 (8): 8192-8206, 2020.
- [2] H.B. Du, B. Yu, J.J. Wei, J. Zhang, D. Wu, W.Q. Tao, Attitude trajectory planning and attitude control for quad-rotor aircraft based on finite-time control technique, *Applied Mathematics and Computation*, 368: 125493, 2020.
- [3] X.L. Shao, X.H. Yue, J. li, Event-triggered robust control for quadrotors with preassigned time performance constraints, *Applied Mathematics and Computation*, (2020) DOI: 10.1016/j.amc.2020.125667.
- [4] J.H. Wang, Y.L. Xu, Y. Xu, D.D. Yang, Time-varying formation for high-order multi-agent systems with external disturbances by event-triggered integral sliding mode control, *Applied Mathematics and Computation*, 359: 333-343, 2019.
- [5] K.Q. Mei, L. Ma, R.X. He, S.H. Ding, Finite-time controller design of multiple integrator nonlinear systems with input saturation, *Applied Mathematics and Computation*, 372: 124986, 2020.
- [6] P.S. Gohari, H. Mohammadi, S. Taghvaei, Using chaotic maps for 3D boundary surveillance by quadrotor robot, *Applied Soft Computing*, 76: 66-77, 2019.
- [7] T. Tomic, K. Schmid, P. Lutz, A. Domel, M. Kassecker, E. Mair, I.L. Grixia, F. Ruess, M. Suppa, D. Burschka, Toward a fully autonomous UAV research platform for indoor and outdoor urban search and rescue, *IEEE Robotics and Automation Magazine*, 19 (3): 46-56, 2012.
- [8] L.H. Qian, H.H.T. Liu, Path-following control of a quadrotor UAV with a cable-suspended payload under wind disturbances, *IEEE Transactions on Industrial Electronics*, 67 (3): 2021-2029, 2020.
- [9] S. Fari, X.M. Wang, S. Roy, S. Baldi, Addressing unmodeled path-following dynamics via adaptive vector field: A UAV Test Case, *IEEE Transactions on Aerospace and Electronic Systems*, 56 (2): 1613-1622, 2020.
- [10] A. Eskandarpour, I. Sharf, A constrained error-based MPC for path following of quadrotor with stability analysis, *Nonlinear Dynamics*, 99 (2): 899-918, 2020.
- [11] X.L. Shao, J. Liu, H.L. Wang, Robust back-stepping output feedback trajectory tracking for quadrotors via extended state observer and sigmoid tracking differentiator, *Mechanical Systems and Signal Processing*, 104: 631-647, 2018.
- [12] L. Zhao, L.W. Dai, Y.Q. Xia, P. Li, Attitude control for quadrotors subjected to wind disturbances via active disturbance rejection control and integral sliding mode control, *Mechanical Systems and Signal Processing*, 129: 531-545, 2019.
- [13] K. Zhao, J.H. Zhang, D.L. Ma, Y.Q. Xia, Composite disturbance rejection attitude control for quadrotor with unknown disturbance, *IEEE Transactions on Industrial Electronics*, 67 (8): 6894-6903, 2020.
- [14] H. Rios, J. Gonzalez-Sierra, A. Dzul, Robust tracking output-control for a quad-rotor: A continuous sliding-mode approach, *Journal of the Franklin Institute-Engineering and Applied Mathematics*, 354 (15): 6672-6691, 2017.
- [15] H. Rios, R. Falcon, O.A. Gonzalez, A. Dzul, Continuous sliding-modes control strategies for quadrotor robust tracking: real-time application, *IEEE Transactions on Industrial Electronics*, 66 (2): 1264-1272, 2019.
- [16] H. Abaunza, P. Castillo, Quadrotor aggressive deployment, using a quaternion-based spherical chattering-free sliding-mode controller, *IEEE Transactions on Aerospace and Electronic Systems*, 56 (3): 1979-1991, 2020.
- [17] X.L. Shao, J. Liu, H.L. Cao. Robust dynamic surface trajectory tracking control for a quadrotor UAV via extended state observer, *International Journal of Robust and Nonlinear Control*, 28(7): 2700-2719, 2018.
- [18] A. Abadi, A. El Amraoui, H. Mekki, N. Ramdani, Robust tracking control of quadrotor based on flatness and active disturbance rejection control, *IET Control Theory and Applications*, 14 (8): 1057-1068, 2020.
- [19] X.L. Shao, Z.L. Cao, H.N. Si, Neurodynamic formation maneuvering control with modified prescribed performances for networked uncertain quadrotors. *IEEE Systems Journal*, (2020) DOI: 10.1109/JSYST.2020.3022901.
- [20] C.X. Mu, Y. Zhang, Learning-based robust tracking control of quadrotor with time-varying and coupling uncertainties, *IEEE Transactions on Neural Networks and Learning Systems*, 31 (1): 259-273, 2020.
- [21] Q.Z. Xu, Z.S. Wang, Z.Y. Zhen, Adaptive neural network finite time control for quadrotor UAV with unknown input saturation, *Nonlinear Dynamics*, 98 (3): 1973-1998, 2019.
- [22] J. Wu, X.M. Chen, Q.J. Zhao, J. Li, and Z.-G. Wu, Adaptive neural dynamic surface control with prespecified tracking accuracy of uncertain stochastic nonstrict-feedback systems, *IEEE Transactions on Cybernetics*, (2020) DOI: 10.1109/TCYB.2020.3012607.
- [23] J.S. Cervantes-Rojas, F. Munoz, I. Chairez, I. Gonzalez-Hernandez, and S. Salazar, Adaptive tracking control of an unmanned aerial system based on a dynamic neural-fuzzy disturbance estimator, *ISA Transactions*, 101: 309-326, 2020.
- [24] Z. Chen, F.H. Huang, W.C. Sun, J. Gu, and B. Yao, RBF-neural-network-based adaptive robust control for nonlinear bilateral teleoperation manipulators with uncertainty and time delay, *IEEE-ASME Transactions on Mechatronics*, 25 (2): 906-918, 2020.
- [25] X.W. Bu, X.Y. Wu, D.Z. Wei, and J.Q. Huang, Neural-approximation-based robust adaptive control of flexible air-breathing hypersonic vehicles with parametric uncertainties and control input constraints, *Information Sciences*, 346: 29-43, 2016.
- [26] B. Xu, P.C. Zhang, Minimal-learning-parameter technique based adaptive neural sliding mode control of MEMS gyroscope, *Complexity*, 6019175, 2017.
- [27] C.P. Bechlioulis, G.A. Rovithakis, Robust adaptive control of feedback linearizable MIMO nonlinear systems with prescribed performance, *IEEE Transactions on Automatic Control*, 53 (9): 2090-2099, 2008.
- [28] F. Mehdifar, C.P. Bechlioulis, F. Hashemzadeh, M. Baradarannia, Prescribed performance distance-based formation

control of multi-agent systems, *Automatica*, (2020) DOI: 10.1016/j.automatica.2020.109086.

- [29] X.W. Bu, Y. Xiao, K. Wang, A prescribed performance control approach guaranteeing small overshoot for air-breathing hypersonic vehicles via neural approximation, *Aerospace Science and Technology*, 71: 485-498, 2017.
- [30] N. Koksai, H. An, B. Fidan, Backstepping-based adaptive control of a quadrotor UAV with guaranteed tracking performance, *ISA transactions*, (2020) DOI: 10.1016/j.isatra.2020.06.006.
- [31] S.L. Dai, S.D. He, X. Chen, X. Jin, Adaptive leader-follower formation control of nonholonomic mobile robots with prescribed transient and steady-state performance, *IEEE Transactions on Industrial Informatics*, 16 (6): 3662-3671, 2020.
- [32] Z.Y. Yin, A. Suleman, J.J. Luo, C.S. Wei, Appointed-time prescribed performance attitude tracking control via double performance functions, *Aerospace Science and Technology*, 93: 105337, 2019.
- [33] C.S. Wei, J.J. Luo, Z.Y. Yin, J.P. Yuan, Leader-following consensus of second-order multi-agent systems with arbitrarily appointed-time prescribed performance, *IET Control Theory and Applications*, 12(16): 2276-2286, 2018.
- [34] X.L. Shao, Y. Shi, Neural adaptive control for MEMS gyroscope with full-state constraints and quantized input, *IEEE Transactions on Industrial Informatics*, 16(10): 6444-6454, 2020.
- [35] X.L. Shao, Y. Shi, W.D. Zhang, H.L. Cao, Neurodynamic approximation-based quantized control with improved transient performances for MEMS gyroscopes: theory and experimental results, *IEEE Transactions on Industrial Electronics*, (2020) DOI: 10.1109/TIE.2020.3026297.
- [36] B. Guo, Y. Chen, Event-triggered robust adaptive sliding mode fault-tolerant control for nonlinear systems, *IEEE Transactions on Industrial Informatics*, 16 (11): 6982-6992, 2020.
- [37] D.Y. Yao, H.Y. Li, R.Q. Lu, Y. Shi, Distributed sliding-mode tracking control of second-order nonlinear multiagent systems: an event-triggered approach, *IEEE Transactions on Cybernetics*, 50 (9): 3892-3902.
- [38] M.G. Lv, D. Wang, Z.H. Peng, L. Liu, H.L. Wang, Event-triggered neural network control of autonomous surface vehicles over wireless network, *Science China-Information Sciences*, 63(5): 150205, 2020.
- [39] X.L. Shao, Y. Shi, W.D. Zhang, Input-and-Measurement event-triggered control for Flexible-Air Breathing Hypersonic Vehicles with asymmetric partial-state constraints, *Nonlinear Dynamics*, (2020) DOI: 10.1007/s11071-020-05942-7.
- [40] Q.X. Yu, Z.S. Hou, X.H. Bu, Q.F. Yu, RBFNN-based data-driven predictive iterative learning control for nonaffine nonlinear systems, *IEEE Transactions on Neural Networks and Learning Systems*, 31(4): 1170-1182, 2020.
- [41] L.D. Su, A radial basis function (RBF)-finite difference (FD) method for the backward heat conduction problem, *Applied Mathematics and Computation*, 354: 232-247, 2019.
- [42] N. Koksai, H. An, B. Fidan, Backstepping-based adaptive control of a quadrotor UAV with guaranteed tracking performance, *ISA transactions*, (2020) DOI:10.1016/j.isatra.2020.06.006.
- [43] F. Mehdifar, C.P. Bechlioulis, F. Hashemzadeh, M. Baradarannia, Prescribed performance distance-based formation control of multi-agent Systems, *Automatica*, 119: 109086, 2020.
- [44] K. Elikier, S. Grouni, M. Tadjine, W.D. Zhang, Practical finite time adaptive robust flight control system for quad-copter UAVs, *Aerospace Science and Technology*, (2020) DOI: 10.1016/j.ast.2020.105708.
- [45] R. Falcon, H. Rios, M. Mera, A. Dzul, Attractive ellipsoid-based robust control for quadrotor tracking, *IEEE Transactions on Industrial Electronics*, 67(9): 7851-7860, 2020.
- [46] X.L. Shao, L.W. Wang, J. Li, J. Liu, High-order ESO based output feedback dynamic surface control for quadrotors under position constraints and uncertainties, *Aerospace Science and Technology*, 89: 288-298, 2019.
- [47] X.N. Xia, and T.P. Zhang, Robust adaptive quantized DSC of uncertain pure-feedback nonlinear systems with time-varying output and state constraints, *International Journal of Robust and Nonlinear Control*, 28 (10): 3357-3375, 2018.
- [48] C. Xi, J. Dong, Adaptive fuzzy guaranteed performance control for uncertain nonlinear systems with event-triggered input, *Applied Mathematics and Computation*, 363: 124604, 2019.
- [49] Y. Huang, J. Wang, D. Shi, and L. Shi, Toward event-triggered extended state observer, *IEEE Transactions of Automatic Control*, 63(6): 1842-1849, 2018.
- [50] X.W. Bu, X.Y. Wu, J.Q. Huang, Z. Ma, R. Zhang, Minimal-learning-parameter based simplified adaptive neural backstepping control of flexible air-breathing hypersonic vehicles without virtual controllers, *Neurocomputing*, 175: 816-825, 2016.
- [51] Z.H. Peng, D. Wang, W. Wang, L. Liu, Containment control of networked autonomous underwater vehicles: A predictor-based neural DSC design, *ISA Transactions*, 59: 160-171, 2015.
- [52] Z.P. Shen, F. Li, X.M. Cao, C. Guo, Prescribed performance dynamic surface control for trajectory tracking of quadrotor UAV with uncertainties and input constraints, *International Journal of Control*, (2020), DOI: 10.1080/00207179.2020.1743366.